

Learning Discretized Neural Networks under Ricci Flow

Jun Chen

*Institute of Cyber-Systems and Control
Zhejiang University
Hangzhou, 310027, China*

JUNC@ZJU.EDU.CN

Hanwen Chen

*Institute of Cyber-Systems and Control
Zhejiang University
Hangzhou, 310027, China*

CHENHANWEN@ZJU.EDU.CN

Mengmeng Wang

*Institute of Cyber-Systems and Control
Zhejiang University
Hangzhou, 310027, China*

MENGMENGWANG@ZJU.EDU.CN

Yong Liu

*Institute of Cyber-Systems and Control
Zhejiang University
Hangzhou, 310027, China*

YONGLIU@IPC.ZJU.EDU.CN

Abstract

In this paper, we consider Discretized Neural Networks (DNNs) consisting of low-precision weights and activations, which suffer from either infinite or zero gradients caused by the non-differentiable discrete function in the training process. In this case, most training-based DNNs use the standard Straight-Through Estimator (STE) to approximate the gradient w.r.t. discrete value. However, the standard STE will cause the gradient mismatch problem, i.e., the approximated gradient direction may deviate from the steepest descent direction. In other words, the gradient mismatch implies the approximated gradient with perturbations. To address this problem, we introduce the duality theory to regard the perturbation of the approximated gradient as the perturbation of the metric in Linearly Nearly Euclidean (LNE) manifolds. Simultaneously, under the Ricci-DeTurck flow, we prove the dynamical stability and convergence of the LNE metric with the L^2 -norm perturbation, which can provide a theoretical solution for the gradient mismatch problem. In practice, we also present the steepest descent gradient flow for DNNs on LNE manifolds from the viewpoints of the information geometry and mirror descent. The experimental results on various datasets demonstrate that our method achieves better and more stable performance for DNNs than other representative training-based methods.

Keywords: Discretized Neural Networks, Ricci Flow, Information Geometry

1. Introduction

Discretized neural networks (Courbariaux et al., 2016; Li et al., 2016; Zhu et al., 2016) have been proven to be efficient in computing, which can significantly reduce computational complexity, storage space, power consumption, resources, etc (Chen et al., 2020). There are roughly two categories of training-based DNNs according to the back-propagation mechanism, i.e., STE and Non-STE methods. The concept of STE was first proposed by Hinton to

penetrate the discrete function in back-propagation (Hinton, 2012), and the following definition of STE was then given by Bengio (Bengio et al., 2013). The key idea of STE can be summarized as: the gradient $\partial L/\partial \hat{\mathbf{a}}$ w.r.t. the discretized neuron can be approximated by the gradient $\partial L/\partial \mathbf{a}$ w.r.t. the non-discretized neuron with clipping, which builds a bridge between the training of neural networks and discretized neural networks¹. Non-STE methods are referred to obtain the feasible discretization without STE, e.g., (Hou et al., 2016; Bai et al., 2018; Leng et al., 2018). However, the learning process for “Non-STE” methods suffers from heavy hyper-parameters (Chen et al., 2019), such as weight partition portion in each iteration (Zhou et al., 2017) and penalty setting in tuning (Leng et al., 2018).

Although STE methods are widely used in DNNs from the view of simplicity and versatility, STE methods almost suffer from a significant drop in accuracy, which is largely caused by the gradient mismatch problem (Cai et al., 2017; Liu et al., 2018; Qin et al., 2020). This problem will affect the training stability of DNNs, which causes DNNs to deviate from the steepest descent direction so that DNNs fall into local optimal points in the training. Since Hubara et al. apply STE to binarized neural networks (Hubara et al., 2016), a series of works are addressing the gradient mismatch problem (Zhou et al., 2016; Chen et al., 2019; Ajanthan et al., 2021). However, from the perspective of the gradient mismatch problem, the mechanism of this problem has not been completely explored yet. Thereby, this paper will focus on the theoretical analysis of the gradient mismatch problem in DNNs, and the corresponding solution is given based on the theoretical exploration.

1.1 Contributions

In this paper, we present an effective solution for the gradient mismatch problem deduced from the viewpoint of duality theory (Amari and Nagaoka, 2000; Amari, 2016), i.e., the perturbation of the approximated gradient caused by the STE in the Euclidean space can be regarded as the perturbation of the metric in the Riemannian manifold². Naturally, we introduce a partial differential equation, i.e., Ricci flow (Sheridan and Rubinstein, 2006), which can converge the initial metric with a small perturbation. Then the perturbation of the approximated gradient caused by the STE can be dynamically decayed by the Ricci flow equation.

The main contributions of this paper are summarized in the following four aspects:

- We propose the LNE manifold endowed with the LNE metric, i.e., a special form of Ricci-flat metrics. According to the information geometry (Amari, 2016) and the mirror descent (Bubeck et al., 2015), we construct LNE manifolds for neural networks.
- We prove the stability of LNE manifolds under the Ricci-DeTurck flow with the L^2 -norm perturbation. In this way, any Ricci-DeTurck flow that starting close to the LNE metric exists for all time, and the Ricci-DeTurck flow will converge to the LNE metric, i.e., the L^2 -norm perturbation of the LNE metric can be dynamically decayed by the Ricci-DeTurck flow.

1. In this paper, the non-discretized neuron is relative to the neural network (its data type is full-precision). And the discretized neuron is relative to the discretized neural network (its data type is low-precision).
 2. This idea is similar to the natural gradient (Martens, 2020).

- Based on the dynamical stability of the Ricci flow, we propose the Ricci Flow Discretized Neural Network (RF-DNN) in the LNE manifold on which we present the weakly and strongly approximated gradient flow, using the STE. It is an effective solution for the gradient mismatch problem in back-propagation.
- We also carry out the experiment on several classification benchmark datasets and network structures. Experimental results demonstrate the effectiveness of our geometric method RF-DNN compared with other representative training-based methods.

1.2 The Following Organization

This paper is organized as follows. In Section 2, we present the related work about the gradient mismatch problem. In Section 3, we introduce the Ricci flow and the motivation for RF-DNNs. According to the geometric structure measured by the LNE divergence, we deduce the corresponding LNE manifold for neural networks in Section 4. The stability of LNE manifolds under the Ricci-DeTurck is proved in Section 5. In Section 6, we give the approximated gradient flow and the constraints of the Ricci flow for RF-DNNs. The experimental results and ablation studies for RF-DNNs are presented in Section 7. Section 8 concludes the entire paper. Proofs are provided in the Appendices.

2. Related Work

2.1 Background

We start with the basic background for feed-forward DNNs that will be used throughout the paper. As for the back-propagation of DNNs, we explain it in later sections.

For a neural network, it can be regarded as a function to transform the input \mathbf{a}_0 to the output \mathbf{a}_l through l layers, with two units in each layer. The first unit outputs a weighted sum of the input \mathbf{a}_{i-1} , and the second unit computes the output of the first unit via a nonlinear function. For the i -th layer ($i \in \{1, 2, \dots, l\}$), we denote \mathbf{W}_i as the weight matrix, \mathbf{s}_i as the vector of these weighted sum and \mathbf{a}_i as the vector of output (also known as the activation).

For a DNN, we need to add a discrete function $Q(*)$ to discretize the weight matrix \mathbf{W}_i and the activation vector \mathbf{a}_i on the basis of neural networks. Furthermore, we mark the discretized weight matrix as $\hat{\mathbf{W}}_i = Q(\mathbf{W}_i)$ and the discretized activation vector as $\hat{\mathbf{a}}_i = Q(\mathbf{a}_i)$. The feed-forward of DNNs at each layer is given as follows:

$$\begin{aligned}
 \mathbf{s}_i &= \hat{\mathbf{W}}_i \otimes \hat{\mathbf{a}}_{i-1} \\
 \mathbf{a}_i &= f \odot \mathbf{s}_i \\
 \hat{\mathbf{a}}_i &= Q(\mathbf{a}_i)
 \end{aligned} \tag{1}$$

where f is a nonlinear function, \odot represents the element-wise multiplication and \otimes represents the convolution. We vectorize $\hat{\mathbf{W}}_i$ as $\text{vec}(\hat{\mathbf{W}}_i)$ and stack their columns together, where $\text{vec}(*)$ is the operator that vectorizes a matrix as a column vector. We define the new discretized parameter vector as $\hat{\boldsymbol{\xi}} = \left[\text{vec}(\hat{\mathbf{W}}_1)^\top, \text{vec}(\hat{\mathbf{W}}_2)^\top, \dots, \text{vec}(\hat{\mathbf{W}}_l)^\top \right]^\top$, where we

ignore the bias vector for convenience. Similarly, we can denote the parameter vector as $\boldsymbol{\xi} = \left[\text{vec}(\mathbf{W}_1)^\top, \text{vec}(\mathbf{W}_2)^\top, \dots, \text{vec}(\mathbf{W}_l)^\top \right]^\top$ where $\hat{\boldsymbol{\xi}} = Q(\boldsymbol{\xi})$.

In frequentist statistics, we represent the loss function as the negative of log likelihood w.r.t. discretized parameter $\hat{\boldsymbol{\xi}}$, where the input $\mathbf{x} = \mathbf{a}_0$ can be observed. The way we minimize the loss function is to maximize the likelihood:

$$L(\mathbf{y}, \mathbf{z}) = -\log p(\mathbf{y}|\mathbf{z}, \hat{\boldsymbol{\xi}}) \quad (2)$$

where \mathbf{y} is the target and \mathbf{z} is the prediction computed by DNNs. In general, \mathbf{z} is the vector of \mathbf{a}_l after the softmax function. Note that $p(\mathbf{y}|\mathbf{z}, \hat{\boldsymbol{\xi}})$ is the probability density function defined by the conditional probability distribution $P_{\mathbf{y}|\mathbf{z}}(\hat{\boldsymbol{\xi}})$ of DNNs.

2.2 Gradient Mismatch

To ensure relatively stable discretization in the training, Hubara et al. applied STE to binarized neural networks as it provides an approximated gradient:

$$\frac{\partial L}{\partial \mathbf{W}} = \frac{\partial L}{\partial Q(\mathbf{W})} \cdot \mathbb{I}, \quad \text{where } \frac{\partial Q(\mathbf{W})}{\partial \mathbf{W}} = \mathbb{I} = \begin{cases} 1 & \text{if } |\mathbf{W}| \leq 1 \\ 0 & \text{otherwise} \end{cases}, \quad (3)$$

where \mathbb{I} is the indicator function. And STE had been successfully implemented in the training of binarized neural networks (Hubara et al., 2016). Li et al. extended STE to ternary neural networks (Li et al., 2016). Subsequently, STE is extended to arbitrary bit-width discretized neural networks (Zhou et al., 2016). However, due to stochastic sampling of the bit, STE methods will bring the gradient mismatch problem inevitably, which almost suffers from a significant drop in accuracy.

There are few works to investigate how to estimate better gradient under the back-propagation mechanism. To explore the solution of gradient mismatch, Zhou et al. proposed to transform \mathbf{W} to $\tilde{\mathbf{W}}$ first:

$$\tilde{\mathbf{W}} = \frac{\tanh(\mathbf{W})}{\max(|\tanh(\mathbf{W})|)}. \quad (4)$$

And then STE acts on the discretized $\tilde{\mathbf{W}}$ (Zhou et al., 2016). During back-propagation, the gradient can be further computed as follows

$$\frac{\partial L}{\partial \mathbf{W}} = \frac{\partial L}{\partial Q(\tilde{\mathbf{W}})} \frac{1 - \tanh^2(\mathbf{W})}{\max(|\tanh(\mathbf{W})|)}. \quad (5)$$

But, the new nonlinear transformation (\tanh) only provides a smooth transition near ± 1 to avoid abrupt clipping of the indicator function, which can not alleviate the gradient mismatch problem. Subsequently, Chen et al. proposed to learn $\partial L / \partial \mathbf{W}$ by a neural network (Chen et al., 2019), e.g., fully-connected layers or LSTM (Sak et al., 2014). Their specific approach is to use neural networks as a shared meta quantizer M_ϕ parameterized by ϕ across layers to replace the gradient via:

$$\frac{\partial L}{\partial \mathbf{W}} = M_\phi \left(\frac{\partial L}{\partial Q(\bar{\mathbf{W}})}, Q(\bar{\mathbf{W}}) \right) \frac{\partial \bar{\mathbf{W}}}{\partial \mathbf{W}}, \quad (6)$$

where \overline{W} is the weight from the meta quantizer. However, with the introduction of new neural networks, the additional errors are also introduced to the gradient propagation, it will further intensify the gradient mismatch problem.

Recently, Ajanthan et al. introduced a mirror descent framework for discretizing neural networks by providing a theoretical framework to perform gradient descent in the dual space with gradients computed in the primal space (Ajanthan et al., 2021), which is strikingly analogous to STE in non-Euclidean spaces. But, this theoretical framework can not provide an effective solution for the gradient mismatch problem.

Motivated from the mirror descent discretization (Ajanthan et al., 2021), in this paper, we consider introducing the Ricci flow into non-Euclidean spaces to form dynamically stable Riemannian manifolds. Using the STE in such time-dependent manifolds, it provides a promised theoretical investigation for gradient match in discretized neural networks.

3. Ricci Flow

The concept of Ricci flow first published by Hamilton (Hamilton et al., 1982) on the manifold \mathcal{M} of a time-dependent Riemannian metric $g(t)$ with the initial metric g_0 :

$$\begin{aligned} \frac{\partial}{\partial t} g(t) &= -2 \text{Ric}(g(t)) \\ g(0) &= g_0 \end{aligned} \tag{7}$$

where Ric denotes the Ricci curvature tensor whose definition can be found in Appendix A.

The purpose of Ricci flow is to prove Thurston’s Geometrization Conjecture and Poincaré Conjecture, which is to evolve the metric that makes the manifold become “round”. Here, the “round” means that the solution of Ricci flow will not shrink to a point, but converge to a constant circle. Thus, the metric will evolve towards certain geometric structures and topological properties (Sheridan and Rubinstein, 2006).

Theorem 1 *When $u : \mathcal{M} \times [0, T) \rightarrow \mathcal{E}$ is a time-dependent section of the vector bundle \mathcal{E} where \mathcal{M} is a Riemannian manifold, if the system of the Ricci flow is strongly parabolic at u_0 then there exists a solution on the time interval $[0, T)$, and the solution is unique for as long as it exists.*

Proof The proofs can be found in (Ladyzhenskaia et al., 1988). ■

Based on Theorem 1, we can know whether there exists a unique solution of Ricci flow for a short time by checking the strongly parabolic. Note that we use the Einstein summation convention (for example, $(AB)_i^j = A_i^k B_k^j$).

Definition 2 *The Ricci flow is strongly parabolic if there exists $\delta > 0$ such that for all covectors $\varphi \neq 0$ and all symmetric $h_{ij} = \frac{\partial g_{ij}(t)}{\partial t} \neq 0$, the principal symbol of -2Ric satisfies*

$$[-2 \text{Ric}](\varphi)(h)_{ij} h^{ij} = g^{pq} (\varphi_p \varphi_q h_{ij} + \varphi_i \varphi_j h_{pq} - \varphi_q \varphi_i h_{jp} - \varphi_q \varphi_j h_{ip}) h^{ij} > \delta \varphi_k \varphi^k h_{rs} h^{rs}.$$

Since the inequality cannot always be satisfied, Ricci flow is not strongly parabolic, which makes us unable to prove the existence of the solution based on Theorem 1. However, it is

possible to understand which parts have an impact on its non-parabolic by the linearization of the Ricci curvature tensor.

Lemma 3 *The linearization of -2Ric can be rewritten as*

$$D[-2 \text{Ric}](h)_{ij} = g^{pq} \nabla_p \nabla_q h_{ij} + \nabla_i V_j + \nabla_j V_i + O(h_{ij})$$

$$\text{where } V_i = g^{pq} \left(\frac{1}{2} \nabla_i h_{pq} - \nabla_q h_{pi} \right). \quad (8)$$

Proof The proofs can be found in Appendix C.1. ■

The term $O(h_{ij})$ will have no contributions to the principal symbol of -2Ric , so we can ignore it in this problem. By carefully observing the above equation, the impact on the non-parabolic of Ricci flow comes from the terms V_i and V_j , instead of the term $g^{pq} \nabla_p \nabla_q h_{ij}$.

Using a time-dependent diffeomorphism $\varphi(t) : \mathcal{M} \rightarrow \mathcal{M}$ (with $\varphi(0) = \text{id}$), the pullback metrics $g(t)$ based on the pull back map φ^* can be expressed as

$$g(t) = \varphi^*(t) \bar{g}(t), \quad (9)$$

which satisfies the Ricci flow equation. Furthermore, the terms V_i and V_j can be reparameterized by choosing $\varphi(t)$ to form the Ricci-DeTurck flow that is strongly parabolic. The solution is followed by the DeTurck Trick (DeTurck, 1983) that has a time-dependent reparameterization of the manifold:

$$\frac{\partial}{\partial t} \bar{g}(t) = -2 \text{Ric}(\bar{g}(t)) - \mathcal{L}_{\frac{\partial \varphi(t)}{\partial t}} \bar{g}(t)$$

$$\bar{g}(0) = \bar{g}_0 + d, \quad (10)$$

where d is a symmetric (0,2)-tensor on \mathcal{M} . See Appendix C.2 for details. Thus, the Ricci-DeTurck flow has a unique solution for a short time. For the long time behavior, please refer to Appendix C.3.

3.1 Stability of Ricci Flow

For the Riemannian n -dimensional manifold (\mathcal{M}^n, g) that is isometric to the Euclidean n -dimensional space (\mathbb{R}^n, δ) , Schnürer et al. (Schnürer et al., 2007) have showed the stability of Euclidean space under the Ricci flow for a small C^0 perturbation. Koch et al. (Koch and Lamm, 2012) have given the stability of the Euclidean space along with the Ricci flow in the L^∞ -norm. Moreover, for the decay of the L^∞ -norm on Euclidean space, Appleton (Appleton, 2018) has given the proof of a different method.

For a Ricci-flat metric with small perturbations, Guenther et al. (Guenther et al., 2002) proved that such metrics would converge under Ricci flow. Considering the stability of integrable and closed Ricci-flat metrics, Sesum (Sesum, 2006) has proved that the convergence rate is exponential because the spectrum of the Lichnerowicz operator is discrete. Furthermore, Deruelle et al. (Deruelle and Kröncke, 2021) have proved that an asymptotically locally Euclidean Ricci-flat metric is dynamically stable under the Ricci flow, with the $L^2 \cap L^\infty$ perturbation on non-flat and non-compact Ricci-flat manifolds.

3.2 Motivation for Ricci Flow Discretized Neural Networks

A series of above proofs about the stability illustrates that the Ricci flow can decay a small perturbation of the metric. Based on the viewpoint of duality theory, we can utilize the Ricci flow to decay the perturbation of the approximated gradient in discretized neural networks.

Now that there are already many stability proofs about near Euclidean metrics under the Ricci flow, why can't we apply it directly to alleviate the gradient mismatch problem? The most fundamental problem is that it is difficult for us to construct such manifolds (e.g. Ricci-flat manifolds) for neural networks. Therefore, we propose a novel LNE manifold differentiated from existing Ricci-flat manifolds. Motivated from the perspective of information geometry, then we can conveniently construct the LNE manifold for a neural network. By proving that a small perturbation of the LNE metric under the Ricci flow is decayed, we thus get a promised theoretical solution for the gradient mismatch problem in DNNs.

4. Neural Networks in LNE Manifolds

Motivated by the previous work (Ajanthan et al., 2021), we introduce the information geometry (Amari and Nagaoka, 2000; Amari, 2016) and the mirror descent algorithm (Bubeck et al., 2015) to construct LNE manifolds for neural networks, as measured by divergences.

4.1 Neural Network Manifold of Positive Measures

A neural network is accompanied by the dynamics of information processing composed of a large number of neurons connected with each other. The set of all such networks forms a manifold, where the weights represented by the neuron connections can be regarded as the coordinate system.

For the $n \times n$ matrix, all such matrices form an n^2 -dimensional manifold. Specifically, the matrix forms the $n(n+1)/2$ -dimensional manifold, i.e., a submanifold embedded in the manifold of all the matrices when this matrix is symmetric and positive-definite. Since symmetric and positive-definite matrices have many advantages, which lead to wide implementations in many fields, our method will also introduce the symmetric and positive-definite matrices in neural networks.

Remark: Comparing straight lines in Euclidean space, geodesics are the straightest possible lines that we can draw in a Riemannian manifold. Given a geodesic, there exists a unique non-Euclidean coordinate system. Once the curved non-Euclidean coordinate system is selected, the symmetric and positive-definite matrix is also represented as a metric in geometry theory. That geometry-based metric can describe the properties of manifolds, such as curvature (Helgason, 2001).

4.2 Euclidean Space and Divergence

From the viewpoints of the information geometry and the mirror descent algorithm, the metric can be deduced by the divergence satisfying the certain criteria (Basseville, 2013), which is summarized as Definition 4. Consequently, we consider two nearby points P and Q in a manifold \mathcal{M} , where these two points are expressed in coordinates as ξ_P and ξ_Q (they are both column vectors). Then, the divergence is defined as half the square of an

infinitesimal distance ds^2 between two sufficiently close points:

$$ds^2 = 2D[\boldsymbol{\xi}_P : \boldsymbol{\xi}_P + d\boldsymbol{\xi}]. \quad (11)$$

Definition 4 $D[P : Q]$ is called a divergence when it satisfies the following criteria:

- (1) $D[P : Q] \geq 0$,
- (2) $D[P : Q] = 0$ when and only when $P = Q$,
- (3) When P and Q are sufficiently close, by denoting their coordinates by $\boldsymbol{\xi}_P$ and $\boldsymbol{\xi}_Q = \boldsymbol{\xi}_P + d\boldsymbol{\xi}$, the Taylor expansion of the divergence can be written as

$$D[\boldsymbol{\xi}_P : \boldsymbol{\xi}_P + d\boldsymbol{\xi}] = \frac{1}{2} \sum_{i,j} g_{ij}(\boldsymbol{\xi}_P) d\xi_i d\xi_j + O(|d\boldsymbol{\xi}|^3), \quad (12)$$

and metric g_{ij} is positive-definite, depending on $\boldsymbol{\xi}_P$.

Using an orthonormal coordinate system in the Euclidean space, a half of the square of the Euclidean distance is naturally defined as the Euclidean divergence between two nearby points $\boldsymbol{\xi}$ and $\boldsymbol{\xi}'$

$$D_E[\boldsymbol{\xi} : \boldsymbol{\xi}'] = \frac{1}{2} \sum_i (\xi_i - \xi'_i)^2. \quad (13)$$

The metric g_{ij} is the Euclidean metric δ_{ij} in this case, so that

$$ds^2 = 2D_E[\boldsymbol{\xi} : \boldsymbol{\xi} + d\boldsymbol{\xi}] = \sum_i (d\xi_i)^2 = \sum_{i,j} \delta_{ij} d\xi_i d\xi_j. \quad (14)$$

Obviously, the Euclidean divergence satisfies the criteria of divergence. Note that the Euclidean metric δ_{ij} is the identity matrix \mathbf{I} where we still retain the notation of metrics because of the representation habit in the geometry theory.

4.3 LNE Manifold and Divergence

In general relativity (Wald, 2010), the complete Riemannian manifold (\mathcal{M}, g) , which is endowed with a linearly nearly flat spacetime metric g_{ij} , is considered to solve the Newtonian limit by linearized gravity. The form of this metric is $g_{ij} = \eta_{ij} + \gamma_{ij}$, where η_{ij} represents a flat Minkowski metric whose background is special relativity and γ_{ij} is smallness. An adequate definition of “smallness” in this context is that the components of γ_{ij} are much smaller than 1 in the global inertial coordinate system of η_{ij} . In practice, this is an excellent theory of small gravitational perturbations when gravity is “weak”.

Similarly, we give a metric $g_{ij} = \delta_{ij} + \gamma_{ij}$ in Riemannian n -manifold (\mathcal{M}^n, g_0) , where δ_{ij} represents a flat Euclidean metric and γ_{ij} is smallness in the global inertial coordinate system of δ_{ij} . The form of the metric is consistent with the LNE metric given in Definition 7. Therefore, we can systematically develop the LNE metric to cope with small perturbations.

4.3.1 CONVEX FUNCTION

In order to construct the LNE manifold endowed with the LNE metric for the neural network, according to Definition 4, we can introduce the divergence to obtain the expression of the LNE metric, similar to the relationship between Euclidean space and divergence.

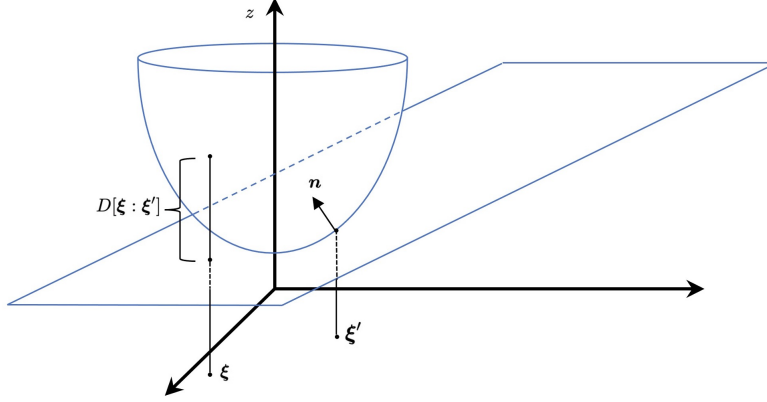


Figure 1: Convex function $z = \phi(\boldsymbol{\xi})$, its supporting hyperplane with normal vector $\mathbf{n} = \nabla\phi(\boldsymbol{\xi})$ and divergence $D[\boldsymbol{\xi} : \boldsymbol{\xi}']$.

There are many applications for different convex functions in physics and optimization. Thus, we can introduce a nonlinear function $\phi(\boldsymbol{\xi})$ of coordinates $\boldsymbol{\xi}$ as the convex function with a certain geometric structure to satisfy the needs of constructing the LNE divergence. When considering a differentiable function, it is said to be convex if and only if its Hessian is positive-definite

$$H(\boldsymbol{\xi}) = \left(\frac{\partial^2}{\partial \xi_i \partial \xi_j} \phi(\boldsymbol{\xi}) \right).$$

4.3.2 LNE DIVERGENCE

By drawing a tangent hyperplane touching it at point $\boldsymbol{\xi}'$

$$z = \phi(\boldsymbol{\xi}') + (\boldsymbol{\xi} - \boldsymbol{\xi}') \nabla \phi(\boldsymbol{\xi}'),$$

we can evaluate the distance between the convex function $\phi(\boldsymbol{\xi})$ and tangent hyperplane z . The graph describing their relationship is shown in Figure 1, where z is the vertical axis of the graph. Since ϕ is convex, the graph of ϕ is always above the hyperplane, touching it at $\boldsymbol{\xi}'$. With a supporting hyperplane of ϕ at $\boldsymbol{\xi}'$, we can deduce the LNE divergence through the Bregman divergence (Bregman, 1967).

Definition 5 *The Bregman divergence (Bregman, 1967) $D_B[\boldsymbol{\xi} : \boldsymbol{\xi}']$ is defined as the difference between a convex function $\phi(\boldsymbol{\xi})$ and its tangent hyperplane $z = \phi(\boldsymbol{\xi}') + (\boldsymbol{\xi} - \boldsymbol{\xi}') \nabla \phi(\boldsymbol{\xi}')$, depending on the Taylor expansion at the point $\boldsymbol{\xi}'$:*

$$D_B[\boldsymbol{\xi} : \boldsymbol{\xi}'] = \phi(\boldsymbol{\xi}) - \phi(\boldsymbol{\xi}') - (\boldsymbol{\xi} - \boldsymbol{\xi}') \nabla \phi(\boldsymbol{\xi}').$$

Geometrically, we propose a symmetrized convex function with the certain geometric structure to construct the LNE divergence based on Definition 5:

$$\phi(\boldsymbol{\xi}) = \sum_i \frac{1}{\tau^2} \log \frac{1}{2} (\exp(\tau \xi_i) + \exp(-\tau \xi_i)) = \sum_i \frac{1}{\tau^2} \log (\cosh(\tau \xi_i)) \quad (15)$$

where τ is a constant parameter.

Theorem 6 For a convex function ϕ defined by Equation (15), the LNE divergence between two points $\boldsymbol{\xi}$ and $\boldsymbol{\xi}'$ is

$$D_{LNE}[\boldsymbol{\xi}' : \boldsymbol{\xi}] = \sum_i \left[\frac{1}{\tau^2} \log \frac{\cosh(\tau \xi'_i)}{\cosh(\tau \xi_i)} - \frac{1}{\tau} (\xi'_i - \xi_i) \tanh(\tau \xi_i) \right] \quad (16)$$

where the Riemannian metric is

$$\begin{aligned} g_0(\boldsymbol{\xi}) &= \delta_{ij} - \left[\tanh(\tau \boldsymbol{\xi}) \tanh(\tau \boldsymbol{\xi})^\top \right]_{ij} \\ &= \begin{bmatrix} 1 - \tanh(\tau \xi_1) \tanh(\tau \xi_1) & \cdots & -\tanh(\tau \xi_1) \tanh(\tau \xi_n) \\ \vdots & \ddots & \vdots \\ -\tanh(\tau \xi_n) \tanh(\tau \xi_1) & \cdots & 1 - \tanh(\tau \xi_n) \tanh(\tau \xi_n) \end{bmatrix}. \end{aligned} \quad (17)$$

Proof The proofs can be found in Appendix G.1. ■

Based on Theorem 6, the form of the metric g_0 constructed by the LNE divergence is consistent with the definition of LNE metrics, as long as we adjust parameter τ to satisfy Definition 7. Moreover, we have also proven that the LNE divergence satisfies the criteria of divergence followed by Definition 4.

Remark: For neural networks, the point (coordinate) $\boldsymbol{\xi}$ is the parameter vector. Therefore, based on Section 4.1, we are able to use the parameters of a neural network to construct the LNE metric. As a result, we can describe the neural network in the LNE manifold, as measured by the LNE divergence based on Theorem 6.

Remark: In fact, the Bregman divergence can be transformed into different forms of the divergence by choosing different convex functions. For example, we can easily obtain the Euclidean divergence from the Bregman divergence, by defining the convex function: $\phi(\boldsymbol{\xi}) = 1/2 \sum_i \xi_i^2$ in a Euclidean space. Besides, given the convex function: $\phi(\boldsymbol{\xi}) = \sum_i p(\mathbf{x}, \xi_i) \log p(\mathbf{x}, \xi_i)$ in a manifold of positive measures where $\sum_i p(\mathbf{x}, \xi_i) = \sum_i p(\mathbf{x}, \xi'_i) = \int p(\mathbf{x}, \boldsymbol{\xi}) d\boldsymbol{\xi} = \int p(\mathbf{x}, \boldsymbol{\xi}') d\boldsymbol{\xi}' = 1$, the Bregman divergence is the same as the KL divergence.

5. Evolution of LNE Manifolds under Ricci Flow

In this section, we will focus on LNE metrics under Ricci flow, and prove that the evolution of LNE manifolds can achieve good performances in terms of stability.

5.1 Analysis on LNE Metrics

For brevity in linearizing, we give the definition of the LNE metric ³ that is a special form of Ricci-flat metrics (Guenther et al., 2002; Deruelle and Kröncke, 2021), which means that the Ricci-flat metrics on noncompact manifolds are LNE. The full statement of the LNE metric is the linearly nearly Euclidean Ricci-flat metric.

Definition 7 A complete Riemannian n -manifold (\mathcal{M}^n, g_0) is said to be LNE with one end of order $\tau > 0$ if there exists a compact set $K \subset \mathcal{M}$, a radius r , a point x in \mathcal{M} and a

3. Its relationship to physics is described in Section 4.3.

diffeomorphism satisfying $\phi : \mathcal{M} \setminus K \rightarrow (\mathbb{R}^n \setminus B(x, r)) / SO(n)$. Note that $B(x, r)$ is the ball and $SO(n)$ is a finite group acting freely on $\mathbb{R}^n \setminus \{0\}$. Then

$$\left| \partial^k (\phi_* \gamma_0) \right|_{\delta} = O(r^{-\tau-k}) \quad \forall k \geq 0 \quad (18)$$

holds on $(\mathbb{R}^n \setminus B(x, r)) / SO(n)$. g_0 can be linearly decomposed into a form containing the Euclidean metric δ :

$$g_0 = \delta + \gamma_0. \quad (19)$$

5.2 Short Time Convergence in the L^2 -norm

In this paper, we consider the linear stability and integrability of the LNE manifold (\mathcal{M}^n, g_0) . Fortunately, similar to the proof process of (Koiso, 1983; Besse, 2007), we can know that (\mathcal{M}^n, g_0) is integral and linearly stable based on Definition 17 and Definition 18.

The main theorem is as follows, whose preparation can be found in Appendix D.

Corollary 8 *Let $(\mathcal{M}^n, \bar{g}_0)$ be the LNE n -manifold. For a Ricci–DeTurck flow $\bar{g}(t)$ on a maximal time interval $t \in [0, T)$, if it satisfies $\|\bar{g}(0) - \bar{g}_0\|_{L^\infty} < \epsilon$ where $\epsilon > 0$, then there exists a constant $C < \infty$ for $t \in (0, T)$. Then we further have*

$$\sup \int_{\mathcal{M}} |d(t)|^2 \kappa^2 d\mu \leq e^{Ct} \sup \int_{\mathcal{M}} |d(0)|^2 \kappa^2 d\mu. \quad (20)$$

Proof The proofs can be found in Appendix F.1. ■

Thus, for the LNE metric with the L^2 -norm perturbation, the Ricci–DeTurck flow in LNE manifolds is stable for a short time.

5.3 Long Time Stability in the L^2 -norm

In order to prove the long time stability of LNE metrics under Ricci–DeTurck flow, we need to construct $\bar{g}_0(t)$ that is a family of Ricci-flat reference metrics with $\frac{\partial}{\partial t} \bar{g}_0(t) = O((\bar{g}(t) - \bar{g}_0(t))^2)$. Let

$$\mathcal{F} = \left\{ \bar{g}(t) \in \mathcal{M}^n \mid 2 \operatorname{Ric}(\bar{g}(t)) + \mathcal{L}_{\frac{\partial \varphi(t)}{\partial t}} \bar{g}(t) = 0 \right\}$$

be the set of stationary points under the Ricci–DeTurck flow. Then, we are able to establish a manifold via an L^2 -neighbourhood \mathcal{U} of integral \bar{g}_0 in the space of metrics

$$\tilde{\mathcal{F}} = \mathcal{F} \cap \mathcal{U}, \quad (21)$$

which is the basis for the later proofs. For all $\bar{g} \in \tilde{\mathcal{F}}$, the terms $\operatorname{Ric}(\bar{g}(t)) = 0$ and $\mathcal{L}_{\frac{\partial \varphi(t)}{\partial t}} \bar{g}(t) = 0$ hold individually, based on the previous work (Deruelle and Kröncke, 2021). In this way, we write $d_0(t) = \bar{g}_0(t) - \bar{g}_0$, so that $d(t) - d_0(t) = \bar{g}(t) - \bar{g}_0(t)$ holds.

The main theorem is as follows, whose preparation can be found in Appendix E.

Theorem 9 *Let $(\mathcal{M}^n, \bar{g}_0)$ be the LNE n -manifold which is linearly stable and integrable. For any metric $\bar{g}(t) \in \mathcal{B}_{L^2}(\bar{g}_0, \epsilon_2)$ where a constant $\epsilon_2 > 0$, there is a complete Ricci–DeTurck flow $(\mathcal{M}^n, \bar{g}(t))$ starting from $\bar{g}(t)$ converging to the LNE metric $\bar{g}(\infty) \in \mathcal{B}_{L^2}(\bar{g}_0, \epsilon_1)$ where ϵ_1 is a small enough constant.*

Proof The proofs can be found in Appendix F.2. ■

We now conclude a result that any Ricci-DeTurck flow that starting close to the LNE metric exists for all time, and the Ricci-DeTurck flow will converge to the LNE metric, i.e., the L^2 -norm perturbation of the LNE metric can be dynamically decayed by the Ricci-DeTurck flow. Thus, the Theorem 9 proves that LNE metrics can achieve good performances in terms of stability under the Ricci-DeTurck flow.

6. Ricci Flow Discretized Neural Networks

We have completed the construction of LNE manifolds for neural networks in Section 4 and analyzed the stability of LNE manifolds under Ricci-DeTurck flow in Section 5. In this section, we propose Ricci flow discretized neural networks (RF-DNNs) to provide an effective solution for the gradient mismatch problem. Then we will focus on how to train the RF-DNN, i.e., computing approximated gradients in LNE manifolds and adding the constraints of the Ricci flow.

By claiming the STE in the Euclidean space, binarized neural networks (Hinton, 2012; Bengio et al., 2013) substituted the standard chain rule with the derivative of identity function multiplied by $\mathbb{I}_{|\mathbf{w}_i| \leq 1}$ in the back-propagation. For training-based RF-DNNs, we will focus on the STE in the LNE manifold.

6.1 Straight-Through Estimator in the Euclidean Space

Using an orthonormal coordinate system in the Euclidean space, the derivative of loss function (2) w.r.t. the discretized parameter vector $\hat{\xi}$ can be computed as the approximated gradient based on the STE, whose negative form represents the direction of the steepest descent. In DNNs, we have

$$\partial_{\xi} L = \partial_{\hat{\xi}} L \cdot \mathbb{I}_{|\xi| \leq 1}. \quad (22)$$

The approximated gradient is defined as the direction in parameter space that gives the largest change in the objective per unit of change in the parameters, as measured by the Euclidean divergence. Note that the derivative w.r.t. the discretized activation vector $\hat{\mathbf{a}}$ can be calculated in a similar way (Hinton, 2012; Bengio et al., 2013). For brevity, we will only discuss the case of weights in later content, where the derivative w.r.t. the discretized activations can be obtained similar to the case of weights.

Remark: By considering a batch of samples instead of all samples in back-propagation, we get the stochastic gradient. Since the essence of the stochastic gradient has not been changed, it can also use the stochastic gradient in the Riemannian manifold.

6.2 Straight-Through Estimator in the LNE Manifold

6.2.1 WEAK APPROXIMATION OF THE GRADIENT FLOW

Based on the LNE divergence in Theorem 6, we consider the approximated gradient for DNNs toward the steepest descent direction on the manifold endowed with LNE metrics:

Lemma 10 *The steepest descent gradient flow measured by the LNE divergence is defined as*

$$\tilde{\partial}_{\boldsymbol{\xi}} = g_0^{-1} \partial_{\boldsymbol{\xi}} = \left[\delta - \tanh(\tau \boldsymbol{\xi}) \tanh(\tau \boldsymbol{\xi})^\top \right]^{-1} \partial_{\boldsymbol{\xi}}. \quad (23)$$

Proof The proofs can be found in Appendix G.2. ■

However, Lemma 10 involves inversion, which greatly consumes computing resources. In particular, we propose two methods for approximating the gradient flow: weak approximation and strong approximation respectively.

The weak approximation of the gradient flow brings higher requirements for those metrics on the basis of Definition 7, i.e., it requires that the LNE metric is also a strictly diagonally-dominant matrix based on Corollary 11.

Corollary 11 *The weak approximation of the gradient flow measured by the LNE divergence is defined as*

$$\tilde{\partial}_{\boldsymbol{\xi}} \approx \left[\delta + \tanh(\tau \boldsymbol{\xi}) \tanh(\tau \boldsymbol{\xi})^\top \right] \partial_{\boldsymbol{\xi}} \quad (24)$$

if the LNE metric g_0 satisfies strictly diagonally-dominant.

Proof The proofs can be found in Appendix G.3. ■

Combined with the STE (22) in the Euclidean space, we can present the weakly approximated STE in the LNE manifold:

$$\tilde{\partial}_{\boldsymbol{\xi}} L \approx \left[\delta + \tanh(\tau \boldsymbol{\xi}) \tanh(\tau \boldsymbol{\xi})^\top \right] \partial_{\boldsymbol{\xi}} L \cdot \mathbb{I}_{|\boldsymbol{\xi}| \leq 1}. \quad (25)$$

In practice, for the layer-by-layer gradient update in back-propagation, we have the weakly approximated STE layer-by-layer in DNNs

$$\tilde{\partial}_{\text{vec}(\mathbf{w}_i)} L \approx (\mathbf{I} + \boldsymbol{\Xi}_i) \partial_{\text{vec}(Q(\mathbf{w}_i))} \cdot \mathbb{I}_{|\text{vec}(\mathbf{w}_i)| \leq 1}. \quad (26)$$

Remark: We mark the block $-\tanh(\tau \boldsymbol{\xi}) \tanh(\tau \boldsymbol{\xi})^\top$ as γ_{ij} and the element $\tanh(\tau \xi_i)$ as ρ_i . For the case of one layer, we rewrite $\text{vec}(\tanh(\tau \mathbf{W}_i)) \text{vec}(\tanh(\tau \mathbf{W}_i))^\top$ as $\boldsymbol{\Xi}_i$.

6.2.2 STRONG APPROXIMATION WITH NEURAL NETWORKS

On the other hand, bypassing the requirement of weak approximation in Corollary 11, our goal is to approximate the gradient flow, $g_0^{-1} \partial_{\boldsymbol{\xi}}$ in Lemma 10, with the assistance of multi-layer perceptron (MLP) neural network. Using the neural network, we can present the strong approximation of the gradient flow as a neural network with a single hidden layer, and a finite number of neurons can be used to approximate a continuous function on compact subsets (Jejjala et al., 2020), which is stated by the universal approximation theorem (Cybenko, 1989; Hornik, 1991).

For the $n \times n$ symmetric matrix, g_0 can be decomposed in terms of the combination of entries P and A , where P is the entries made up of the elements of the lower triangular matrix that contains $n(n-1)/2$ real parameters and A is the entries made up of the elements

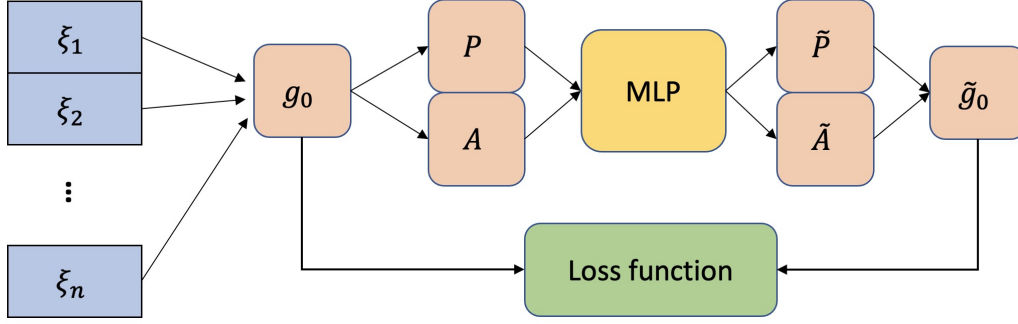


Figure 2: Flow chart of strong approximation of the gradient flow. The new entries \tilde{P} and \tilde{A} produced by neural network get combined into a new metric \tilde{g}_0 that is used to minimize the loss function by combining with the metric g_0 , where the loss function is defined by Equation (27).

of the diagonal matrix that contains n real parameters. After the training in Figure 2, \tilde{g}_0 can be regarded as the strong approximation of the gradient flow g_0^{-1} .

$$L = \|\mathbf{I} - g_0 \tilde{g}_0\|^2. \quad (27)$$

6.3 Ricci Curvature in Neural Networks

For the neural network in the LNE manifold, we can consider the Ricci curvature of the neural network manifold. According to Appendix A, we present

$$\begin{aligned} -2 \operatorname{Ric}(g) &= -2R_{ikj}^i = 2R_{kij}^i \\ &= g^{ip} (\partial_i \partial_k g_{pj} - \partial_i \partial_j g_{pk} + \partial_p \partial_j g_{ik} + \partial_p \partial_k g_{ij}). \end{aligned} \quad (28)$$

Inspired by (Kaul and Lall, 2019), we treat the term i and p as the translation and rotation for each input. As the standard data augmentation can not include the rotation, we only consider the translation instead of the rotation, i.e., $\partial_p (\partial_j g_{ik} + \partial_k g_{ij}) = 0$ for the fairness of ablation studies. Therefore, $\partial_k g$ and $\partial_j g$ can be the row and column transformation of the input data w.r.t. the metric g . Consequently, we have

$$-2 \operatorname{Ric}(g) = g^{ip} \partial_i (\partial_k g_{pj} - \partial_j g_{pk}). \quad (29)$$

Remark: The choice of i and p is arbitrary (including k and j), and can even be other coordinate representations. Here, we just give it a specific geometric meaning by considering the characteristic of the neural network task.

For the computation, we replace partial derivatives with difference equations, i.e., $\partial_k g = (g|_{k1} - g|_{k2}) / (k1 - k2)$ and $\partial_j g = (g|_{j1} - g|_{j2}) / (j1 - j2)$ based on the input translation dimensions k and j respectively. Meanwhile, we discard the term p , as the rotation of the input data is not considered. The Ricci curvature tensor can be further simplified as

$$-2 \operatorname{Ric}(g) = \frac{g|_{k1} - g|_{k2}}{k1 - k2} - \frac{g|_{l1} - g|_{l2}}{l1 - l2}. \quad (30)$$

In general, $(k1 - k2)$ and $(j1 - j2)$ are translations less than 4 pixels, which is consistent with data augmentation.

6.4 Relaxed Regularization and the Existence of Ricci Flow

Recall that we consider the Ricci-DeTurck flow instead of the Ricci flow, as the solution of the Ricci flow does not always exist based on Section 3. However, we can not deal with the Ricci-DeTurck flow in DNNs, as the Ricci-DeTurck flow depends on the choice of $\varphi(t)$. Let us look at this in another way. If we can ensure that the solution of Ricci flow exists, then we can easily consider the Ricci flow in DNNs.

To ensure the existence of the solution of Ricci flow, we require the tensor $-2 \text{Ric}(g)$ will approach zero, as $\frac{\partial}{\partial t}g$ approaches zero ⁴ based on Equation (7). Consequently, we may achieve the goal ($-2 \text{Ric}(g)$ approaches zero) by adding a regularization into the loss function for the RF-DNN. Followed by Equation (30), we then can present the regularization w.r.t. the metrics $g(t)$

$$g(t)_N = \left\| \frac{g(t)|_{k1} - g(t)|_{k2}}{k1 - k2} - \frac{g(t)|_{l1} - g(t)|_{l2}}{l1 - l2} \right\|_{L^2}^2, \quad (31)$$

where $g(t)$ is ϵ -close to g_0 based on Definition 24, which is the necessary condition for the evolution of Ricci flow.

Combined with Equation (50), the upper bound of Equation (31) is estimated by

$$\begin{aligned} g(t)_N &\leq \left\| \frac{(1 + \epsilon)^2 \cdot g_0|_{k1} - g_0|_{k2}}{(1 + \epsilon)(k1 - k2)} - \frac{g_0|_{l1} - (1 + \epsilon)^2 \cdot g_0|_{l2}}{(1 + \epsilon)(l1 - l2)} \right\|_{L^2}^2 \\ &= \frac{1}{1 + \epsilon} \left\| \frac{(1 + \epsilon)^2 \cdot \gamma|_{k1} - \gamma|_{k2}}{k1 - k2} - \frac{\gamma|_{l1} - (1 + \epsilon)^2 \cdot \gamma|_{l2}}{l1 - l2} + \frac{\epsilon^2 + 2\epsilon}{k1 - k2} \delta + \frac{\epsilon^2 + 2\epsilon}{l1 - l2} \delta \right\|_{L^2}^2, \end{aligned} \quad (32)$$

and the lower bound of Equation (31) is estimated by

$$\begin{aligned} g(t)_N &\geq \left\| \frac{g_0|_{k1} - (1 + \epsilon)^2 \cdot g_0|_{k2}}{(1 + \epsilon)(k1 - k2)} - \frac{(1 + \epsilon)^2 \cdot g_0|_{l1} - g_0|_{l2}}{(1 + \epsilon)(l1 - l2)} \right\|_{L^2}^2 \\ &= \frac{1}{1 + \epsilon} \left\| \frac{\gamma|_{k1} - (1 + \epsilon)^2 \cdot \gamma|_{k2}}{k1 - k2} - \frac{(1 + \epsilon)^2 \cdot \gamma|_{l1} - \gamma|_{l2}}{l1 - l2} - \frac{\epsilon^2 + 2\epsilon}{k1 - k2} \delta - \frac{\epsilon^2 + 2\epsilon}{l1 - l2} \delta \right\|_{L^2}^2. \end{aligned} \quad (33)$$

As the evolution of Ricci flow converges, the estimate of Equation (31) tends to be stable:

$$g(t)_N \xrightarrow{\text{Ricci flow}} N = \left\| \frac{\gamma|_{k1} - \gamma|_{k2}}{k1 - k2} - \frac{\gamma|_{l1} - \gamma|_{l2}}{l1 - l2} \right\|_{L^2}^2. \quad (34)$$

For the dynamically stable LNE metric, we can also use the relaxed regularization N with the suitable coefficient α instead of the regularization $g(t)_N$. With the application of the relaxed regularization, we can ensure that the solution of Ricci flow exists when the RF-DNN converges.

4. There are two aspects to explain this reason. On the one hand, the convergence of the Ricci flow requires that the metric g converges. On the other hand, with the convergence of DNNs, the convergence of parameters also causes the metric g composed of parameters to converge.

Remark: In practice, we can compute 4 different parameter vectors $\xi|_{k1}$, $\xi|_{k2}$, $\xi|_{l1}$ and $\xi|_{l2}$ by back-propagating the 4 different translations of input data to obtain $\gamma|_{k1}$, $\gamma|_{k2}$, $\gamma|_{l1}$ and $\gamma|_{l2}$ where the metric $\gamma_{ij} = -\tanh(\tau\xi)\tanh(\tau\xi)^\top$.

6.5 The Algorithm Design

In Equation (26), we obtain the weakly approximated gradient layer-by-layer for DNNs in LNE manifolds. For the gradient of RF-DNNs in LNE manifolds, we need to introduce the constraints of the Ricci flow to Equation (26) additionally.

Based on Equation (30), we present the expression of the discrete Ricci Flow

$$g(t+1)|_{k1} - g(t)|_{k1} = \frac{g(t)|_{k1} - g(t)|_{k2}}{k1 - k2} - \frac{g(t)|_{l1} - g(t)|_{l2}}{l1 - l2}, \quad (35)$$

where the Euclidean metric δ in g has no effect on the Ricci flow. Thus, we can replace the representation of g with γ_{ij} or Ξ_i , where the matrix $\Xi_i = \text{vec}(\tanh(\tau\mathbf{W}_i))\text{vec}(\tanh(\tau\mathbf{W}_i))^\top$ is the decomposition of the metric $-\gamma_{ij}$ layer-by-layer.

By applying the constraints of the discrete Ricci Flow layer-by-layer, we get the final approximated gradient of RF-DNNs via a small constant β

$$\begin{aligned} \tilde{\partial}_{\mathbf{W}_i} L &= \text{mat} \left((\mathbf{I} + \Xi_i(t)) \partial_{\text{vec}(Q(\mathbf{W}_i))} \right) \cdot \tilde{\mathbb{I}} \\ \text{where } \tilde{\mathbb{I}} &= \begin{cases} 1 & \text{if } \left| \Xi_i(t+1)|_{k1} - \Xi_i(t)|_{k1} + \frac{\Xi_i(t)|_{k2} - \Xi_i(t)|_{k1}}{k1 - k2} - \frac{\Xi_i(t)|_{l2} - \Xi_i(t)|_{l1}}{l1 - l2} \right| \leq \beta \\ 0 & \text{otherwise} \end{cases}, \end{aligned} \quad (36)$$

where $\text{mat}(\ast)$ is the reverse operator of $\text{vec}(\ast)$, which turns the column vector back into a matrix. Consequently, under the constraints of the discrete Ricci flow, each back-propagation of RF-DNNs will alleviate the gradient mismatch problem. The overall process is shown in Algorithm 1.

Remark: In addition to using the discretized weight and activation, DNNs need to save the non-discretized weight and activation for gradient update. Note that the gradient of a DNN is non-discretized.

7. Experimental Results

In this section, we design ablation studies to compare our RF-DNN trained from scratch with other STE methods. Furthermore, given a pre-trained model, we evaluate the performance of the RF-DNN in comparison with several representative training-based methods on classification benchmark datasets. All the experiments implemented in Python are conducted with PyTorch (Paszke et al., 2019). The hardware environment is conducted on a Workstation with an Intel(R) Xeon(R) Silver 4214 CPU(2.20 GHz), GeForce GTX 1080Ti GPU and 128GB RAM.

7.1 Experimental Settings

The two datasets used in our experiments are introduced as follows.

CIFAR datasets: There are two CIFAR benchmarks (Krizhevsky et al., 2009) consisting of natural color images with 32×32 pixels, respectively, 50k training and 10k test

Algorithm 1 An algorithm for computing the gradient of the loss function and training our RF-DNN. We choose 4 different translations: $k1, k2, j1$ and $j2$. We define a parameter α for balancing the regularization. For the RF-DNN in the LNE manifold with g_0 , we use $\tilde{\partial}$ as the approximated gradient based on Equation (36). For brevity, we ignore the normalization operation (Ioffe and Szegedy, 2015; Ba et al., 2016).

Input: A minibatch of inputs and targets $(\mathbf{x} = \mathbf{a}_0, \mathbf{y})$, $\boldsymbol{\xi}$ mapped to $(\mathbf{W}_1, \mathbf{W}_2, \dots, \mathbf{W}_l)$, $\hat{\boldsymbol{\xi}}$ mapped to $(\hat{\mathbf{W}}_1, \hat{\mathbf{W}}_2, \dots, \hat{\mathbf{W}}_l)$, a nonlinear function f , a constant factor τ and a learning rate η .

Output: The updated discretized parameters $\hat{\boldsymbol{\xi}}$.

```

1: {Forward propagation}
2: for  $m$  in  $k1, k2, j1, j2$  do
3:   for  $i = 1; i \leq l; i++$  do
4:     Compute  $\hat{\mathbf{W}}_i|_m = Q(\mathbf{W}_i|_m)$ ;
5:     Compute  $\mathbf{s}_i|_m = \hat{\mathbf{W}}_i|_m \otimes \hat{\mathbf{a}}_{i-1}|_m$ ;
6:     Compute  $\hat{\mathbf{a}}_i|_m = Q(f \odot \mathbf{s}_i|_m)$ ;
7:   end for
8:   Compute  $\gamma|_m = -\tanh(\tau\boldsymbol{\xi}|_m)\tanh(\tau\boldsymbol{\xi}|_m)^\top$ ;
9: end for
10: Compute  $N = \left\| \frac{\gamma|_{k1} - \gamma|_{k2}}{k1 - k2} - \frac{\gamma|_{l1} - \gamma|_{l2}}{l1 - l2} \right\|_{L^2}^2$ ;
11: {Loss derivative for  $m = k1$ }
12: Compute  $L = L(\mathbf{y}, \mathbf{z}) + \alpha \cdot N$ ;
13: Compute  $\partial_{\mathbf{a}_i} L = \frac{\partial L(\mathbf{y}, \mathbf{z})}{\partial \mathbf{z}} \Big|_{\mathbf{z}=\hat{\mathbf{a}}_i}$ ;
14: {Backward propagation}
15: for  $i = l; i \geq 1; i--$  do
16:   Compute  $\partial_{\mathbf{s}_i} L = \partial_{\mathbf{a}_i} L \odot f'(\mathbf{s}_i)$ ;
17:   Compute the constraints  $(\tilde{\mathbb{I}})$  of discrete Ricci flow based on Equation (36);
18:   Compute  $\tilde{\partial}_{\mathbf{W}_i} L = \text{mat}((\mathbf{I} + \boldsymbol{\Xi}_i(t)) \text{vec}(\nabla_{\mathbf{s}_i} L \otimes \hat{\mathbf{a}}_{i-1}^\top)) \cdot \tilde{\mathbb{I}}$ ;
19:   Compute  $\partial_{\mathbf{a}_{i-1}} L = (\hat{\mathbf{W}}_i^\top \otimes \partial_{\mathbf{s}_i} L) \cdot \mathbb{I}_{|\mathbf{a}_{i-1}| \leq 1}$ ;
20: end for
21: {The parameters update}
22: for  $i = l; i \geq 1; i--$  do
23:   Update  $\mathbf{W}_i(t+1) = \mathbf{W}_i(t) - \eta \cdot \tilde{\partial}_{\mathbf{W}_i} L$ ;
24:   Compute  $\boldsymbol{\Xi}_i(t+1) = \text{vec}(\tanh(\tau\mathbf{W}_i(t+1))) \text{vec}(\tanh(\tau\mathbf{W}_i(t+1)))^\top$ ;
25: end for
26: Update  $\hat{\boldsymbol{\xi}} = \left[ \text{vec}(Q(\mathbf{W}_1))^\top, \text{vec}(Q(\mathbf{W}_2))^\top, \dots, \text{vec}(Q(\mathbf{W}_l))^\top \right]^\top$ ;

```

images, and we pick out 5k training images as a validation set from the training set. CIFAR-10 consists of images organized into 10 classes and CIFAR-100 into 100 classes. We adopt a standard data augmentation scheme (random corner cropping and random flipping) that is widely used for these two datasets. We normalize the images with the means of the channel and standard deviations in preprocessing.

ImageNet dataset: The ImageNet benchmark (Russakovsky et al., 2015) consists of 1.2 million high-resolution natural images, where the validation set contains 50k images. These images are organized into 1000 categories of the objects for training, which are resized to 224×224 pixels before fed into the network. In the next experiments, we report our single-crop evaluation results using top-1 and top-5 accuracies.

We specify the discrete function, the composition of which has a significant influence on the performance and computation of DNNs. Specifically, a discrete function composed of more discrete values will always achieve better performances, and the operations to simplify the calculations, e.g., fixed-point multiplication, SHIFT operation (Elhoushi et al., 2019) and XNOR operation (Rastegari et al., 2016) etc, are also varied depending on the different discrete values.

We mark Q^1 as the 1-bit discrete function:

$$Q^1(*) = \mathbb{E}[|*|] \cdot \text{sign}(*) = \mathbb{E}[|*|] \cdot \{-1, +1\}. \quad (37)$$

A DNN using discrete function Q^1 can be calculated with XNOR operation. The k -bit, over 1-bit, discrete function can be marked as Q^k ,

$$Q^{k>1}(*) = \text{clip}\left(\frac{1}{2^{k-1}-1} \text{round}\left((2^{k-1}-1) \cdot *\right), -1, +1\right) \quad (38)$$

where $\text{round}(*)$ is the rounding function and $\text{clip}(*, -1, +1)$ is the clipping function that constraints the input to the range of $[-1, +1]$. Then a DNN using discrete function $Q^{k>1}$ can be calculated with fixed-point multiplication.

7.2 Ablation Studies with STE Methods

In order to illustrate the superiority of RF-DNN against the gradient mismatch problem, we compare our RF-DNN with three other methods, i.e., Dorefa (Zhou et al., 2016), MultiFCG (Chen et al., 2019) and FCGrad (Chen et al., 2019), which are all trained from scratch. For these ablation studies, we discretize all layers in the networks with 1-bit using Equation (37). As the factor $\mathbb{E}[|*|]$ can be absorbed into the normalization, the weights can be expressed by -1 or $+1$. Here, we apply different ResNet models (He et al., 2016) to learn the corresponding DNNs.

The batch normalization with a batch size of 128 is used in the learning strategy, and Nesterov momentum of 0.9 (Dozat, 2016) is used in SGD optimization. For CIFAR, we set total training epochs as 200 and set a weight decay of 0.0005 where the learning rate is lowered by 10 times at epoch 80, 150, and 190, with the initial value of 0.1. For ImageNet, we set total training epochs as 100 and set the learning rate of each parameter group using a cosine annealing schedule with a weight decay of 0.0001. All experiments are conducted for 5 times, and the statistics of the last 10/5 epochs' test accuracies are reported for a fair comparison. Note that we perform standard data augmentation and pre-processing on CIFAR and ImageNet datasets.

In Table 1, Table 2 and Table 3, we use the same the discrete function Q^1 , parameter setting and optimizer for fairness in the forward. The only difference is the training method in the backward propagation. The performance in various models and datasets shows that our RF-DNN has significant improvement than other STE methods.

Table 1: The experimental results on CIFAR10 with ResNet20/32/44. The accuracy of full-precision (FP) baseline is reported by (Chen et al., 2019).

Network	Forward	Backward	Test Acc (%)	FP Acc (%)
ResNet20	$\{-1,+1\}$	Dorefa	88.28±0.81	91.50
		MultiFCG	88.94±0.46	
		RF-DNN	89.83±0.23	
ResNet32	$\{-1,+1\}$	Dorefa	90.23±0.63	92.13
		MultiFCG	89.63±0.38	
		RF-DNN	90.75±0.19	
ResNet44	$\{-1,+1\}$	Dorefa	90.71±0.58	93.56
		MultiFCG	90.54±0.21	
		RF-DNN	91.63±0.11	

Table 2: The experimental results on CIFAR100 with ResNet56/110. The accuracy of full-precision (FP) baseline is reported by (Chen et al., 2019).

Network	Forward	Backward	Test Acc (%)	FP Acc (%)
ResNet56	$\{-1,+1\}$	Dorefa	66.71±2.32	71.22
		MultiFCG	66.58±0.37	
		FCGrad	66.56±0.35	
		RF-DNN	68.56±0.32	
ResNet110	$\{-1,+1\}$	Dorefa	68.15±0.50	72.54
		MultiFCG	68.27±0.14	
		FCGrad	68.74±0.36	
		RF-DNN	69.20±0.28	

7.3 Convergence and Stability Analysis

Based on the above ablation studies, we compare the convergence and stability of our RF-DNN and Dorefa during the training and test processes. As shown in Figure 3, the RF-DNN can achieve higher accuracies than Dorefa on CIFAR100 dataset, i.e., 1.25% higher on the training dataset with ResNet56, 1.85% higher on the test dataset with ResNet56, 1.97% higher on the training dataset with ResNet110 and 1.05% higher on the test dataset with ResNet110. In addition, it can be seen from the fluctuation of the test curves in Figure 3 that the RF-DNN has a tremendous improvement compared with the Dorefa on the stability of training.

Table 3: The experimental results on ImageNet with ResNet18. The accuracy of full-precision (FP) baseline is reported by (Chen et al., 2019).

Network	Forward	Backward	Test Top1/Top5 (%)	FP Top1/Top5 (%)
ResNet18	{-1,+1}	Dorefa	58.34±2.07/81.47±1.56	69.76/89.08
		MultiFCG	59.47±0.02/82.41±0.01	
		FCGrad	59.83±0.36/82.67±0.23	
		RF-DNN	60.83±0.41/83.54±0.18	

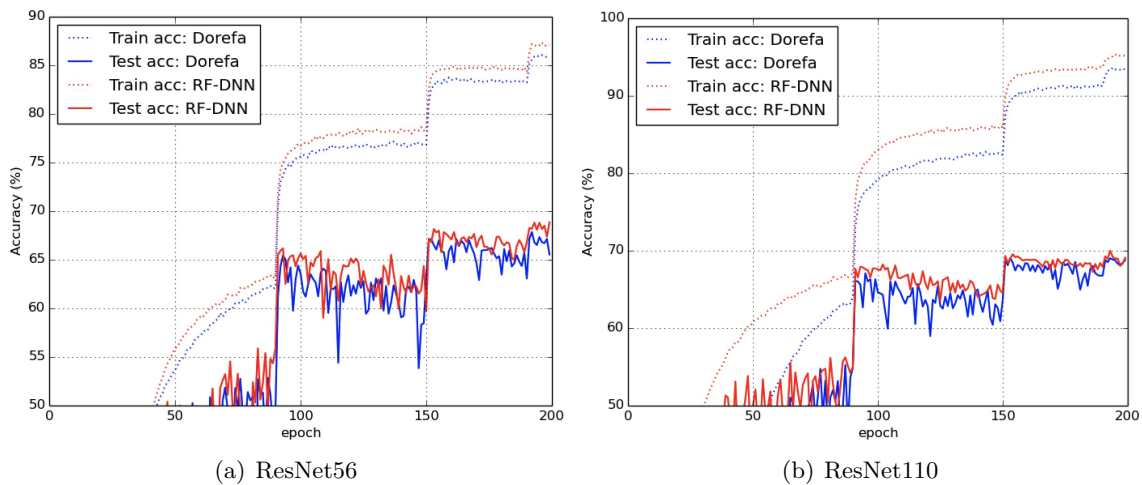


Figure 3: Training and test curves of ResNet56/110 on CIFAR100 compared between Dorefa and RF-DNN.

The ablation studies can exactly verify the viewpoint of duality theory that the DNN with the constraints of the Ricci flow will be an effective solution against the gradient mismatch problem in the LNE manifold.

7.4 Training Time Analysis

In our hardware environment, we record the training time per iteration for our RF-DNN, MultiFCG, and Dorefa with the model of ResNet20 in the CIFAR10 dataset. For each training iteration, our RF-DNN costs 35.34 seconds, MultiFCG costs 18.44 seconds, and Dorefa costs 17.81 seconds. Compared with MultiFCG and Dorefa, our RF-DNN costs more calculation time, and this part of the extra time mainly comes from solving the constraints of the Ricci flow. Although the training time of our RF-DNN is longer, it is acceptable compared to the improvement brought by our method. And our method also has room for parallel optimization, but it is out of the scope of this paper.

Table 4: The classification accuracy results on ImageNet and comparison with other training-based methods, with AlexNet (Krizhevsky et al., 2012), ResNet18, ResNet50 and MobileNet (Howard et al., 2017). Note that the accuracy of full-precision baseline is reported by (Elhoushi et al., 2019).

Method	W	A	Top-1		Top-5	
			Accuracy	Gap	Accuracy	Gap
AlexNet (Original)	32	32	56.52%	-	79.07%	-
RF-DNN (ours)	6	32	56.39%	-0.13%	78.78%	-0.29%
DeepShift (Elhoushi et al., 2019)	6	32	54.97%	-1.55%	78.26%	-0.81%
ResNet18 (Original)	32	32	69.76%	-	89.08%	-
RF-DNN (ours)	1	32	67.05%	-2.71%	88.09%	-0.99%
MD (Ajanthan et al., 2021)	1	32	66.78%	-2.98%	87.01%	-2.07%
ELQ (Zhou et al., 2018)	1	32	66.21%	-3.55%	86.43%	-2.65%
ADMM (Leng et al., 2018)	1	32	64.80%	-4.96%	86.20%	-2.88%
QN (Yang et al., 2019)	1	32	66.50%	-3.26%	87.30%	-1.78%
MetaQuant (Chen et al., 2019)	1	32	63.44%	-6.32%	84.77%	-4.31%
RF-DNN (ours)	4	4	66.75%	-3.01%	87.02%	-2.06%
RQ ST (Louizos et al., 2019)	4	4	62.46%	-7.30%	84.78%	-4.30%
ResNet50 (Original)	32	32	76.13%	-	92.86%	-
RF-DNN (ours)	8	8	76.07%	-0.06%	92.87%	+0.01%
INT8 (Zhu et al., 2020)	8	8	75.87%	-0.26%	-	-
MobileNet (Original)	32	32	70.61%	-	89.47%	-
RF-DNN (ours)	5	5	61.32%	-9.29%	84.08%	-5.39%
SR+DR (Gysel et al., 2018)	5	5	59.39%	-11.22%	82.35%	-7.12%
RQ ST (Louizos et al., 2019)	5	5	56.85%	-13.76%	80.35%	-9.12%
RF-DNN (ours)	8	8	70.76%	+0.15%	89.54%	+0.07%
RQ (Louizos et al., 2019)	8	8	70.43%	-0.18%	89.42%	-0.05%

7.5 Comparisons with Training-based Methods

In this experiment, based on a full-precision pre-trained model, we compare the RF-DNN with several state-of-the-art DNNs, e.g., DeepShift (Elhoushi et al., 2019), QN (Yang et al., 2019), ADMM (Leng et al., 2018), MetaQuant (Chen et al., 2019), INT8 (Zhu et al., 2020), SR+DR (Gysel et al., 2018), ELQ (Zhou et al., 2018), MD (Ajanthan et al., 2021) and RQ (Louizos et al., 2019), under the same bit width using Equation (37) or Equation (38). Note that **W** and **A** represent the bit width of discretized weights and activations respectively in Table 4.

Consequently, the experimental results show that our RF-DNN is able to achieve better performance than other recent state-of-the-art training-based methods, which seems to benefit from our effective solution for the gradient mismatch problem.

8. Conclusion

In this paper, we propose to learn a discretized neural network under Ricci flow, which provides an effective solution for the gradient mismatch problem caused by the standard Straight-Through Estimator. By defining the gradient mismatch problem as the approximated gradient with perturbations, we regard the perturbation of the approximated gradient as perturbations of the metric based on the viewpoint of the duality theory. We then prove the stability of LNE metrics with the L^2 -norm perturbation under Ricci-DeTurck flow in theory. Subsequently, we introduce the Ricci flow to decay the perturbation of the metric for a neural network in the LNE manifold that is constructed by the information geometry and mirror descent. In practice, we propose the Ricci flow Discretized Neural Network (RF-DNN) by using both the approximated gradient flow and the constraints of the Ricci flow in the LNE manifold. Accordingly, our RF-DNN achieves improvements in both the stability and performance of DNNs, which is verified by experimental results.

The future research may focus on describing the neural network on a dynamically stable manifold. And the manifold learning to assist the training of neural networks can be a useful future direction.

Appendix A. Differential Geometry

1. Riemann curvature tensor (Rm) is a (1,3)-tensor defined for a 1-form ω :

$$R_{ijk}^l \omega_l = \nabla_i \nabla_j \omega_k - \nabla_j \nabla_i \omega_k$$

where the covariant derivative of F satisfies

$$\nabla_p F_{i_1 \dots i_k}^{j_1 \dots j_l} = \partial_p F_{i_1 \dots i_k}^{j_1 \dots j_l} + \sum_{s=1}^l F_{i_1 \dots i_k}^{j_1 \dots q \dots j_l} \Gamma_{pq}^{j_s} - \sum_{s=1}^k F_{i_1 \dots q \dots i_k}^{j_1 \dots j_l} \Gamma_{pi_s}^q.$$

In particular, coordinate form of the Riemann curvature tensor is:

$$R_{ijk}^l = \partial_i \Gamma_{jk}^l - \partial_j \Gamma_{ik}^l + \Gamma_{jk}^p \Gamma_{ip}^l - \Gamma_{ik}^p \Gamma_{jp}^l.$$

2. Christoffel symbol in terms of an ordinary derivative operator is:

$$\Gamma_{ij}^k = \frac{1}{2} g^{kl} (\partial_i g_{jl} + \partial_j g_{il} - \partial_l g_{ij}).$$

3. Ricci curvature tensor (Ric) is a (0,2)-tensor:

$$R_{ij} = R_{pij}^p.$$

4. Scalar curvature is the trace of the Ricci curvature tensor:

$$R = g^{ij} R_{ij}.$$

5. Lie derivative of F in the direction $\frac{d\varphi(t)}{dt}$:

$$\mathcal{L}_{\frac{d\varphi(t)}{dt}} F = \left(\frac{d}{dt} \varphi^*(t) F \right)_{t=0}$$

where $\varphi(t) : \mathcal{M} \rightarrow \mathcal{M}$ for $t \in (-\epsilon, \epsilon)$ is a time-dependent diffeomorphism of \mathcal{M} to \mathcal{M} .

Appendix B. Notation

For clarity of definitions in this paper, we list the important notations as shown in Table 5.

Appendix C. Proof for the Ricci Flow

C.1 Proof for Lemma 3

Definition 12 *The linearization of the Ricci curvature tensor is given by*

$$D[\text{Ric}](h)_{ij} = -\frac{1}{2} g^{pq} (\nabla_p \nabla_q h_{ij} + \nabla_i \nabla_j h_{pq} - \nabla_q \nabla_i h_{jp} - \nabla_q \nabla_j h_{ip}).$$

Proof Based on Appendix A, we have

$$\nabla_q \nabla_i h_{jp} = \nabla_i \nabla_q h_{jp} - R_{qij}^r h_{rp} - R_{qip}^r h_{jm}.$$

Table 5: Definitions of notations

\mathbf{W}_i :	weight matrix for the i -th layer	$\hat{\mathbf{W}}_i$:	discretized weight matrix for the i -th layer
\mathbf{a}_i :	activation vector for the i -th layer	$\hat{\mathbf{a}}_i$:	discretized activation vector for the i -th layer
$\boldsymbol{\xi}$:	parameter vector	$\hat{\boldsymbol{\xi}}$:	discretized parameter vector
Q^1 :	1-bit discrete function	$Q^{k>1}$:	k-bit discrete function (over 1-bit)
δ :	Euclidean metric (identity matrix)	g or $g(t)$:	the pullback metrics under Ricci flow
g_0 :	LNE metric under Ricci flow	$g(0)$:	initial metric under Ricci flow
g_x :	a metric for any point $x \in \mathcal{M}$	\bar{g} or $\bar{g}(t)$:	metrics under Ricci-DeTurck flow
$\bar{g}(0)$:	an initial metric under Ricci-DeTurck flow	\bar{g}_0 :	LNE metric under Ricci-DeTurck flow
$\bar{g}_0(t)$:	the family of Ricci-flat metrics	$d(t)$:	the time-dependent difference
$d(0)$:	the initial perturbation	L :	loss function
L_{g_0} :	Lichnerowicz operator	L^2 or L^∞ :	norm
∂ :	partial derivative	∇ :	covariant derivative
\mathcal{L} :	Lie derivative	Δ_{g_0} :	the Laplacian
Rm:	Riemann curvature tensor	Rm $_x$:	Riemann curvature tensor for any point $x \in \mathcal{M}$
Ric:	Ricci curvature tensor	D :	divergence
φ^* :	pull back map	ϕ_* :	push forward map
$D[\text{Ric}]$:	the linearization of the Ricci curvature tensor	$\mathcal{B}_{L^2}(\bar{g}_0, \epsilon)$:	the ϵ -ball with respect to the L^2 -norm induced by \bar{g}_0 and centred at \bar{g}_0
$B(x, r)$:	the ball with a radius r and a point $x \in \mathcal{M}$		

Combining with Definition 12, we can obtain the deformation equation because of $\nabla_k g_{ij} = 0$,

$$\begin{aligned}
 D[-2\text{Ric}](h)_{ij} &= g^{pq} \nabla_p \nabla_q h_{ij} + \nabla_i \left(\frac{1}{2} \nabla_j h_{pq} - \nabla_q h_{jp} \right) + \nabla_j \left(\frac{1}{2} \nabla_i h_{pq} - \nabla_q h_{ip} \right) + O(h_{ij}) \\
 &= g^{pq} \nabla_p \nabla_q h_{ij} + \nabla_i V_j + \nabla_j V_i + O(h_{ij}).
 \end{aligned}$$

■

C.2 Description of the DeTurck Trick

Based on the chain rule for the Lie derivative in Appendix A, we can calculate

$$\begin{aligned}
 \frac{\partial}{\partial t}g(t) &= \frac{\partial(\varphi^*(t)\bar{g}(t))}{\partial t} \\
 &= \left(\frac{\partial(\varphi^*(t+\tau)\bar{g}(t+\tau))}{\partial \tau} \right)_{\tau=0} \\
 &= \left(\varphi^*(t) \frac{\partial \bar{g}(t+\tau)}{\partial \tau} \right)_{\tau=0} + \left(\frac{\partial(\varphi^*(t+\tau)\bar{g}(t))}{\partial \tau} \right)_{\tau=0} \\
 &= \varphi^*(t) \frac{\partial}{\partial t} \bar{g}(t) + \varphi^*(t) \mathcal{L}_{\frac{\partial \varphi(t)}{\partial t}} \bar{g}(t).
 \end{aligned}$$

With the help of Equation (7), we have the following expression for the pullback metric $g(t)$

$$\frac{\partial}{\partial t}g(t) = \varphi^*(t) \frac{\partial}{\partial t} \bar{g}(t) + \varphi^*(t) \mathcal{L}_{\frac{\partial \varphi(t)}{\partial t}} \bar{g}(t) = -2 \text{Ric}(\varphi^*(t)\bar{g}(t)) = -2\varphi^*(t) \text{Ric}(\bar{g}(t)). \quad (39)$$

The diffeomorphism invariance of the Ricci curvature tensor is used in the last step. The above equation is equivalent to

$$\frac{\partial}{\partial t} \bar{g}(t) = -2 \text{Ric}(\bar{g}(t)) - \mathcal{L}_{\frac{\partial \varphi(t)}{\partial t}} \bar{g}(t).$$

C.3 Curvature Explosion at Singularity

In general, we present the behavior of Ricci flow in finite time and show that the evolution of the curvature is close to divergence. The core demonstration is followed with Theorem 16.

Theorem 13 *Given a smooth Riemannian metric g_0 on a closed manifold \mathcal{M} , there exists a maximal time interval $[0, T)$ such that a solution $g(t)$ of the Ricci flow, with $g(0) = g_0$, exists and is smooth on $[0, T)$, and this solution is unique.*

Proof The proofs can be found in (Sheridan and Rubinstein, 2006). ■

Theorem 14 *Let \mathcal{M} be a closed manifold and $g(t)$ a smooth time-dependent metric on \mathcal{M} , defined for $t \in [0, T)$. If there exists a constant $C < \infty$ for all $x \in \mathcal{M}$ such that*

$$\int_0^T \left| \frac{\partial}{\partial t} g_x(t) \right|_{g(t)} dt \leq C, \quad (40)$$

then the metrics $g(t)$ converge uniformly as t approaches T to a continuous metric $g(T)$ that is uniformly equivalent to $g(0)$ and satisfies

$$e^{-C} g_x(0) \leq g_x(T) \leq e^C g_x(0). \quad (41)$$

Proof Considering any $x \in \mathcal{M}$, $t_0 \in [0, T)$, $V \in T_x \mathcal{M}$, we have

$$\begin{aligned} \left| \log \left(\frac{g_x(t_0)(V, V)}{g_x(0)(V, V)} \right) \right| &= \left| \int_0^{t_0} \frac{\partial}{\partial t} [\log g_x(t)(V, V)] dt \right| \\ &= \left| \int_0^{t_0} \frac{\frac{\partial}{\partial t} g_x(t)(V, V)}{g_x(t)(V, V)} dt \right| \\ &\leq \int_0^{t_0} \left| \frac{\partial}{\partial t} g_x(t) \left(\frac{V}{|V|_{g(t)}}, \frac{V}{|V|_{g(t)}} \right) \right| dt \\ &\leq \int_0^{t_0} \left| \frac{\partial}{\partial t} g_x(t) \right|_{g(t)} dt \\ &\leq C. \end{aligned}$$

By exponentiating both sides of the above inequality, we have

$$e^{-C} g_x(0)(V, V) \leq g_x(t_0)(V, V) \leq e^C g_x(0)(V, V).$$

This inequality can be rewritten as

$$e^{-C} g_x(0) \leq g_x(t_0)(V, V) \leq e^C g_x(0)(V, V)$$

because it holds for any V . Thus, the metrics $g(t)$ are uniformly equivalent to $g(0)$.

Consequently, we have the well-defined integral:

$$g_x(T) - g_x(0) = \int_0^T \frac{\partial}{\partial t} g_x(t) dt.$$

We can show that this integral is well-defined from two perspectives. Firstly, as long as the metrics are smooth, the integral exists. Secondly, the integral is absolutely integrable. Based on the norm inequality induced by $g(0)$, we can obtain

$$|g_x(T) - g_x(t)|_{g(0)} \leq \int_t^T \left| \frac{\partial}{\partial t} g_x(t) \right|_{g(0)} dt.$$

For each $x \in \mathcal{M}$, the above integral will approach zero as t approaches T . Since \mathcal{M} is compact, the metrics $g(t)$ converge uniformly to a continuous metric $g(T)$ which is uniformly equivalent to $g(0)$ on \mathcal{M} . Moreover, we can show that

$$e^{-C} g_x(0) \leq g_x(T) \leq e^C g_x(0).$$

■

Corollary 15 *Let $(\mathcal{M}, g(t))$ be a solution of the Ricci flow on a closed manifold. If $|\text{Rm}|_{g(t)}$ is bounded on a finite time $[0, T)$, then $g(t)$ converges uniformly as t approaches T to a continuous metric $g(T)$ which is uniformly equivalent to $g(0)$.*

Proof The bound on $|\text{Rm}|_{g(t)}$ implies one on $|\text{Ric}|_{g(t)}$. Based on Equation (7), we can extend the bound on $|\frac{\partial}{\partial t}g(t)|_{g(t)}$. Therefore, we obtain an integral of a bounded quantity over a finite interval is also bounded, by Theorem 14. \blacksquare

Theorem 16 *If g_0 is a smooth metric on a compact manifold \mathcal{M} , the Ricci flow with $g(0) = g_0$ has a unique solution $g(t)$ on a maximal time interval $t \in [0, T)$. If $T < \infty$, then*

$$\lim_{t \rightarrow T} \left(\sup_{x \in \mathcal{M}} |\text{Rm}_x(t)| \right) = \infty. \quad (42)$$

Proof For a contradiction, we assume that $|\text{Rm}_x(t)|$ is bounded by a constant. It follows from Corollary 15 that the metrics $g(t)$ converges smoothly to a smooth metric $g(T)$. Based on Theorem 13, it is possible to find a solution to the Ricci flow on $t \in [0, T)$, as the smooth metric $g(T)$ is uniformly equivalent to the initial metric $g(0)$.

Hence, we can extend the solution of the Ricci flow after the time point $t = T$, which contradicts the choice of T as the maximal time for the existence of the Ricci flow on $[0, T)$. In other words, $|\text{Rm}_x(t)|$ is unbounded. \blacksquare

As approaching the singular time T , the Riemann curvature $|\text{Rm}|_{g(t)}$ becomes no longer convergent and tends to explode.

Appendix D. Proof for Short Time Convergence in LNE Manifolds

Definition 17 *A complete LNE n -manifold (\mathcal{M}^n, g_0) is said to be linearly stable if the L^2 spectrum of the Lichnerowicz operator $L_{g_0} := \Delta_{g_0} + 2\text{Rm}(g_0)*$ is in $(-\infty, 0]$ where Δ_{g_0} is the Laplacian, when L_{g_0} acting on d_{ij} satisfies*

$$\begin{aligned} L_{g_0}(d) &= \Delta_{g_0}d + 2\text{Rm}(g_0)*d \\ &= \Delta_{g_0}d + 2\text{Rm}(g_0)_{iklj}d_{mn}g_0^{km}g_0^{ln}. \end{aligned} \quad (43)$$

Definition 18 *A n -manifold (\mathcal{M}^n, g_0) is said to be integrable if a neighbourhood of g_0 has a smooth structure.*

We rewrite the Ricci-DeTurck flow (10) in terms of the difference $d(t) := \bar{g}(t) - \bar{g}_0$, such that

$$\begin{aligned} \frac{\partial}{\partial t}d(t) &= \frac{\partial}{\partial t}\bar{g}(t) = -2\text{Ric}(\bar{g}(t)) + 2\text{Ric}(\bar{g}_0) + \mathcal{L}_{\frac{\partial \varphi'(t)}{\partial t}}\bar{g}_0 - \mathcal{L}_{\frac{\partial \varphi(t)}{\partial t}}\bar{g}(t) \\ &= \Delta d(t) + \text{Rm} * d(t) + F_{\bar{g}^{-1}} * \nabla^{\bar{g}_0} d(t) * \nabla^{\bar{g}_0} d(t) + \nabla^{\bar{g}_0} (G_{\Gamma(\bar{g}_0)} * d(t) * \nabla^{\bar{g}_0} d(t)), \end{aligned} \quad (44)$$

where the tensors F and G depend on \bar{g}^{-1} and $\Gamma(\bar{g}_0)$. Note that \bar{g}_0 is the LNE metric which satisfies the above formula.

In the following, we denote $\|\cdot\|_{L^2}$ or $\|\cdot\|_{L^\infty}$ as the L^2 -norm or L^∞ -norm w.r.t. the LNE metric \bar{g}_0 , and mark generic constants as C or C_1 .

Lemma 19 *Let $(\mathcal{M}^n, \bar{g}_0)$ be a complete Ricci-flat n -manifold. If $\bar{g}(0)$ is a metric satisfying $\|\bar{g}(0) - \bar{g}_0\|_{L^\infty} < \epsilon$ where $\epsilon > 0$, then there exists a constant $C < \infty$ and a unique Ricci-DeTurck flow $\bar{g}(t)$ that satisfies*

$$\|\bar{g}(t) - \bar{g}_0\|_{L^\infty} < C\|\bar{g}(0) - \bar{g}_0\|_{L^\infty} < C \cdot \epsilon. \quad (45)$$

Proof The same statement is given in (Deruelle and Kröncke, 2021). The proofs can refer the details (Bamler, 2010, 2011). \blacksquare

Lemma 20 *Let $(\mathcal{M}^n, \bar{g}_0)$ be the LNE n -manifold. For a Ricci-DeTurck flow $\bar{g}(t)$ on a maximal time interval $t \in [0, T)$, if it satisfies $\|\bar{g}(0) - \bar{g}_0\|_{L^\infty} < \epsilon$ where $\epsilon > 0$, then there exists a constant $C < \infty$ for $t \in (0, T)$ such that*

$$\|\bar{g}(t) - \bar{g}_0\|_{L^2} \leq C. \quad (46)$$

Proof Based on Lemma 19, we can consider $\|\bar{g}(t) - \bar{g}_0\|_{L^2}$. Let κ be a function such that $\kappa = 1$ on $B(x, r)$, $\kappa = 0$ on $\mathcal{M}^n \setminus B(x, 2r)$ and $|\nabla \kappa| \leq 2/r$ where $x \in \mathcal{M}^n$ and a radius r .

Followed by Equation (44), we obtain

$$\begin{aligned} \frac{\partial}{\partial t} \int_{\mathcal{M}} |d(t)|^2 \kappa^2 d\mu &\leq 2 \int_{\mathcal{M}} \langle \Delta d(t), \kappa^2 d(t) \rangle d\mu + C \|\text{Rm}\|_{L^\infty} \int_{\mathcal{M}} |d(t)|^2 \kappa^2 d\mu \\ &\quad + C \|d(t)\|_{L^\infty} \int_{\mathcal{M}} |\nabla d(t)|^2 \kappa^2 d\mu + \int_{\mathcal{M}} \langle \nabla(G_\Gamma * d * \nabla d), d \rangle \kappa^2 d\mu \\ &\leq -2 \int_{\mathcal{M}} |\nabla d(t)|^2 \kappa^2 d\mu + C \int_{\mathcal{M}} |\nabla d(t)| |d(t)| |\nabla \kappa| \kappa d\mu \\ &\quad + C(\bar{g}_0) \int_{\mathcal{M}} |d(t)|^2 \kappa^2 d\mu + C \|d(t)\|_{L^\infty} \int_{\mathcal{M}} |\nabla d(t)|^2 \kappa^2 d\mu \\ &\leq (-2 + C \cdot \epsilon + C_1) \int_{\mathcal{M}} |\nabla d(t)|^2 \kappa^2 d\mu + C(\bar{g}_0) \int_{\mathcal{M}} |d(t)|^2 \kappa^2 d\mu \\ &\quad + \frac{1}{C_1} \int_{\mathcal{M}} |d(t)|^2 |\nabla \kappa|^2 d\mu \\ &\leq \left(C(\bar{g}_0) + \frac{2}{C_1 r^2} \right) \int_{B(x, 2r)} |d(t)|^2 d\mu. \end{aligned}$$

Note that we can always find a suitable C_1 to make the above formula true. By integration in time t , we can further obtain

$$\int_{\mathcal{M}} |d(t)|^2 \kappa^2 d\mu \leq \int_{\mathcal{M}} |d(0)|^2 \kappa^2 d\mu + \left(C(\bar{g}_0) + \frac{2}{C_1 r^2} \right) \int_0^t \int_{B(x, 2r)} |d(s)|^2 d\mu ds < \infty.$$

Consequently, we can find a finite ball that satisfies this estimate. \blacksquare

Appendix E. Proof for Long Time Stability in LNE Manifolds

Lemma 21 *Let $\bar{g}(t)$ be a Ricci–DeTurck flow on a maximal time interval $t \in (0, T)$ in an L^2 -neighbourhood of \bar{g}_0 . We have the following estimate:*

$$\left\| \frac{\partial}{\partial t} d_0(t) \right\|_{L^2} \leq C \left\| \nabla^{\bar{g}_0(t)} (d(t) - d_0(t)) \right\|_{L^2}^2. \quad (47)$$

Proof According to the Hardy inequality (Minerbe, 2009), we have the same proofs by referring the details (Deruelle and Kröncke, 2021). \blacksquare

Theorem 22 *Let $(\mathcal{M}^n, \bar{g}_0)$ be the LNE n -manifold which is linearly stable and integrable. Then, there exists a constant $\alpha_{\bar{g}_0}$ satisfying*

$$(\Delta d(t) + \text{Rm}(\bar{g}_0) * d(t), d(t))_{L^2} \leq -\alpha_{\bar{g}_0} \left\| \nabla^{\bar{g}_0} d(t) \right\|_{L^2}^2 \quad (48)$$

for all $\bar{g}(t) \in \tilde{\mathcal{F}}$ whose definition is given in Equation (21).

Proof The similar proofs can be found in (Devyver, 2014) with some minor modifications. Due to the linear stability requirement of LNE manifolds in Definition 17, $-L_{\bar{g}_0}$ is non-negative. Then there exists a positive constant $\alpha_{\bar{g}_0}$ satisfying

$$\alpha_{\bar{g}_0} (-\Delta d(t), d(t))_{L^2} \leq (-\Delta d(t) - \text{Rm}(\bar{g}_0) * d(t), d(t))_{L^2}.$$

By Taylor expansion, we repeatedly use elliptic regularity and Sobolev embedding (Pacini, 2010) to obtain the estimate. \blacksquare

Corollary 23 *Let $(\mathcal{M}^n, \bar{g}_0)$ be the LNE n -manifold which is integrable. For a Ricci–DeTurck flow $\bar{g}(t)$ on a maximal time interval $t \in [0, T]$, if it satisfies $\|\bar{g}(t) - \bar{g}_0\|_{L^\infty} < \epsilon$ where $\epsilon > 0$, then there exists a constant $C < \infty$ for $t \in [0, T]$ such that the evolution inequality satisfies*

$$\|d(t) - d_0(t)\|_{L^2}^2 \geq C \int_0^t \left\| \nabla^{\bar{g}_0(s)} (d(s) - d_0(s)) \right\|_{L^2}^2 dt. \quad (49)$$

Proof Based on Equation (44), we know

$$\begin{aligned} \frac{\partial}{\partial t} (d(t) - d_0) &= \Delta(d(t) - d_0) + \text{Rm} * (d(t) - d_0) \\ &\quad + F_{\bar{g}^{-1}} * \nabla^{\bar{g}_0} (d(t) - d_0) * \nabla^{\bar{g}_0} (d(t) - d_0) \\ &\quad + \nabla^{\bar{g}_0} (G_{\Gamma(\bar{g}_0)} * (d(t) - d_0) * \nabla^{\bar{g}_0} (d(t) - d_0)). \end{aligned}$$

Followed by Lemma 21 and Theorem 22, we further obtain

$$\begin{aligned}
 \frac{\partial}{\partial t} \|d(t) - d_0\|_{L^2}^2 &= 2(\Delta(d(t) - d_0) + \text{Rm} * (d(t) - d_0), d(t) - d_0)_{L^2} \\
 &\quad + (F_{\bar{g}^{-1}} * \nabla^{\bar{g}_0}(d(t) - d_0) * \nabla^{\bar{g}_0}(d(t) - d_0), d(t) - d_0)_{L^2} \\
 &\quad + (\nabla^{\bar{g}_0}(G_{\Gamma(\bar{g}_0)} * (d(t) - d_0) * \nabla^{\bar{g}_0}(d(t) - d_0)), d(t) - d_0)_{L^2} \\
 &\quad + \left(d(t) - d_0, \frac{\partial}{\partial t} d_0(t) \right)_{L^2} + \int_{\mathcal{M}} (d(t) - d_0) * (d(t) - d_0) * \frac{\partial}{\partial t} d_0(t) d\mu \\
 &\leq -2\alpha_{\bar{g}_0} \|\nabla^{\bar{g}_0}(d(t) - d_0)\|_{L^2}^2 \\
 &\quad + C \|d(t) - d_0\|_{L^\infty} \|\nabla^{\bar{g}_0}(d(t) - d_0)\|_{L^2}^2 \\
 &\quad + \left\| \frac{\partial}{\partial t} d_0(t) \right\|_{L^2} \|d(t) - d_0\|_{L^2} \\
 &\leq (-2\alpha_{\bar{g}_0} + C \cdot \epsilon) \|\nabla^{\bar{g}_0}(d(t) - d_0)\|_{L^2}^2.
 \end{aligned}$$

Let ϵ be a small enough constant that $-2\alpha_{\bar{g}_0} + C \cdot \epsilon < 0$ holds, we can find

$$\frac{\partial}{\partial t} \|d(t) - d_0\|_{L^2}^2 \leq -C \|\nabla^{\bar{g}_0}(d(t) - d_0)\|_{L^2}^2$$

holds. ■

Definition 24 Let $\bar{g}(t)$ be the metrics on the LNE manifold. For $\epsilon > 0$, $\mathcal{B}_{L^2}(\bar{g}_0, \epsilon)$ is the ϵ -ball with respect to the L^2 -norm induced by \bar{g}_0 and centred at \bar{g}_0 , where any metric $\bar{g}(t) \in \mathcal{B}_{L^2}(\bar{g}_0, \epsilon)$ is ϵ -close to \bar{g}_0 if

$$(1 + \epsilon)^{-1} \bar{g}_0 \leq \bar{g}(t) \leq (1 + \epsilon) \bar{g}_0 \tag{50}$$

in the sense of matrices.

Appendix F. Proof for Evolution of LNE Manifolds under Ricci Flow

F.1 Proof for Corollary 8

Based on Lemma 20, we obtain

$$\begin{aligned}
 \sup \int_{\mathcal{M}} |d(t)|^2 \kappa^2 d\mu &\leq \sup \int_{\mathcal{M}} |d(0)|^2 \kappa^2 d\mu \\
 &\quad + N \left(C(\bar{g}_0) + \frac{2}{C_1 r^2} \right) \int_0^t \sup \int_{\mathcal{M}} |d(s)|^2 \kappa^2 d\mu ds,
 \end{aligned}$$

where each ball of radius $2r$ on \mathcal{M} can be covered by N balls of radius r because $(\mathcal{M}^n, \bar{g}_0)$ is LNE. By the Gronwall inequality, we have

$$\sup \int_{\mathcal{M}} |d(t)|^2 \kappa^2 d\mu \leq \exp \left(N \left(C(\bar{g}_0) + \frac{2}{C_1 r^2} \right) t \right) \sup \int_{\mathcal{M}} |d(0)|^2 \kappa^2 d\mu.$$

F.2 Proof for Theorem 9

By Lemma 19, we have a constant $\epsilon_2 > 0$ such that $d(t) \in \mathcal{B}_{L^2}(0, \epsilon_2)$ holds. By Lemma 21 (in the second step) and Corollary 23 (in the third step), we can obtain

$$\begin{aligned} \|d_0(T)\|_{L^2} &\leq C \int_1^T \left\| \frac{\partial}{\partial t} d_0(t) \right\|_{L^2} dt \\ &\leq C \int_1^T \|\nabla^{\bar{g}_0} (d(t) - d_0(t))\|_{L^2}^2 dt \\ &\leq C \|d(1) - d_0(1)\|_{L^2}^2 \leq C \|d(1)\|_{L^2}^2 \leq C \cdot (\epsilon_2)^2. \end{aligned}$$

Furthermore, we can obtain from the above formulas

$$\|d(T) - d_0(T)\|_{L^2} \leq \|d(1) - d_0(1)\|_{L^2} \leq C \cdot \epsilon_2.$$

By the triangle inequality, we get

$$\|d(T)\|_{L^2} \leq C \cdot (\epsilon_2)^2 + C \cdot \epsilon_2.$$

Followed by Corollary 8 and Lemma 21, T should be pushed further outward, i.e.,

$$\limsup_{t \rightarrow +\infty} \left\| \frac{\partial}{\partial t} d_0(t) \right\|_{L^2} \leq \limsup_{t \rightarrow +\infty} \|\nabla^{\bar{g}_0} (d(t) - d_0(t))\|_{L^2}^2 = 0.$$

Thus, $\bar{g}(t)$ will converge to $\bar{g}(\infty) = \bar{g}_0 + d_0(\infty)$ as t approaches $+\infty$ based on the elliptic regularity. In other words, $d(t) - d_0(t)$ will converge to 0 as t goes to $+\infty$ w.r.t. all Sobolev norms (Minerbe, 2009),

$$\lim_{t \rightarrow +\infty} \|d(t) - d_0(t)\|_{L^2} \leq \lim_{t \rightarrow +\infty} C \|\nabla^{\bar{g}_0} (d(t) - d_0(t))\|_{L^2} = 0.$$

Appendix G. Proof for the Information Geometry

G.1 Proof for Theorem 6

The LNE divergence can be defined between two nearby points ξ and ξ' , where the first derivative of the LNE divergence w.r.t. ξ' is:

$$\begin{aligned} &\partial_{\xi'} D_{LNE}[\xi' : \xi] \\ &= \sum_i \left[\partial_{\xi'_i} \frac{1}{\tau^2} \log \cosh(\tau \xi'_i) - \partial_{\xi'_i} \frac{1}{\tau^2} \log \cosh(\tau \xi_i) - \frac{1}{\tau} \partial_{\xi'_i} (\xi'_i - \xi_i) \tanh(\tau \xi_i) \right] \\ &= \sum_i \partial_{\xi'_i} \frac{1}{\tau^2} \log \cosh(\tau \xi'_i) - \frac{1}{\tau} \tanh(\tau \xi). \end{aligned}$$

The second derivative of the LNE divergence w.r.t. ξ' is:

$$\partial_{\xi'}^2 D_{LNE}[\xi' : \xi] = \sum_i \partial_{\xi'_i}^2 \frac{1}{\tau^2} \log \cosh(\tau \xi'_i).$$

We deduce the Taylor expansion of the LNE divergence at $\xi' = \xi$:

$$\begin{aligned}
 D_{LNE}[\xi' : \xi] &\approx D_{LNE}[\xi : \xi] + \left(\sum_i \partial_{\xi'_i} \frac{1}{\tau^2} \log \cosh(\tau \xi'_i) - \frac{1}{\tau} \tanh(\tau \xi) \right) \Big|_{\xi'=\xi}^\top d\xi \\
 &+ \frac{1}{2} d\xi^\top \left(\sum_i \partial_{\xi'_i}^2 \frac{1}{\tau^2} \log \cosh(\tau \xi'_i) \right) \Big|_{\xi'=\xi} d\xi \\
 &= 0 + 0 + \frac{1}{2\tau^2} d\xi^\top \partial \left[\frac{\partial \cosh(\tau \xi)}{\cosh(\tau \xi)} \right] d\xi \\
 &= \frac{1}{2\tau^2} d\xi^\top \frac{\partial^2 \cosh(\tau \xi) \cosh(\tau \xi) - \partial \cosh(\tau \xi) \partial \cosh(\tau \xi)^\top}{\cosh^2(\tau \xi)} d\xi \\
 &= \frac{1}{2\tau^2} d\xi^\top \left(\frac{\partial^2 \cosh(\tau \xi)}{\cosh(\tau \xi)} - \tau^2 \left[\frac{\sinh(\tau \xi)}{\cosh(\tau \xi)} \right] \left[\frac{\sinh(\tau \xi)}{\cosh(\tau \xi)} \right]^\top \right) d\xi \\
 &= \frac{1}{2} \sum_{i,j} \delta_{ij} - \left[\tanh(\tau \xi) \tanh(\tau \xi)^\top \right]_{ij} d\xi_i d\xi_j.
 \end{aligned}$$

G.2 Proof for Lemma 10

We would like to know in which direction minimizes the loss function with the constraints of the LNE divergence, so that we do the minimization:

$$d\xi^* = \underset{d\xi \text{ s.t. } D_{LNE}[\xi:\xi+d\xi]=c}{\arg \min} L(\xi + d\xi)$$

where c is the constant. The loss function descends along the manifold with constant speed, regardless the curvature.

Furthermore, we can write the minimization in Lagrangian form. Combined with Theorem 6, the LNE divergence can be approximated by its second order Taylor expansion. Approximating $L(\xi + d\xi)$ with its first order Taylor expansion, we get:

$$\begin{aligned}
 d\xi^* &= \arg \min_{d\xi} L(\xi + d\xi) + \lambda (D_{LNE}[\xi : \xi + d\xi] - c) \\
 &\approx \arg \min_{d\xi} L(\xi) + \partial_\xi L(\xi)^\top d\xi + \frac{\lambda}{2} d\xi^\top g_0 d\xi - c\lambda.
 \end{aligned}$$

To solve this minimization, we set its derivative w.r.t. $d\xi$ to zero:

$$\begin{aligned}
 0 &= \frac{\partial}{\partial d\xi} L(\xi) + \partial_\xi L(\xi)^\top d\xi + \frac{\lambda}{2} d\xi^\top \left[\delta - \tanh(\tau \xi) \tanh(\tau \xi)^\top \right] d\xi - c\lambda \\
 &= \partial_\xi L(\xi) + \lambda \left[\delta - \tanh(\tau \xi) \tanh(\tau \xi)^\top \right] d\xi \\
 d\xi &= -\frac{1}{\lambda} \left[\delta - \tanh(\tau \xi) \tanh(\tau \xi)^\top \right]^{-1} \partial_\xi L(\xi)
 \end{aligned}$$

where a constant factor $1/\lambda$ can be absorbed into learning rate. Therefore, we get the optimal descent direction, i.e., the opposite direction of gradient, which takes into account the local curvature defined by $[\delta - \tanh(\tau \xi) \tanh(\tau \xi)^\top]^{-1}$.

G.3 Proof for Corollary 11

Definition 25 For $A \in \mathcal{R}^{n \times n}$, A is called as the strictly diagonally-dominant matrix when it satisfies

$$|a_{ii}| > \sum_{j=1, j \neq i}^n |a_{ij}|, \quad i = 1, 2, \dots, n.$$

Definition 26 If $A \in \mathcal{R}^{n \times n}$ is a strictly diagonally-dominant matrix, then A is a nonsingular matrix together.

Subsequently, we can consider the inverse matrix of the LNE metric g_0 . Due to the strictly diagonally-dominant feature in Definition 25 and Definition 26, we can approximate $[\delta - \tanh(\tau\xi) \tanh(\tau\xi)^\top]^{-1}$. Furthermore, we can also ignore the fourth-order small quantity $\sum O(\rho_a \rho_b \rho_c \rho_d)$

$$\begin{aligned} & [\delta - \tanh(\tau\xi) \tanh(\tau\xi)^\top]^{-1} [\delta + \tanh(\tau\xi) \tanh(\tau\xi)^\top] \\ &= \begin{bmatrix} 1 - \rho_1 \rho_1 & -\rho_1 \rho_2 & \cdots \\ -\rho_2 \rho_1 & 1 - \rho_2 \rho_2 & \cdots \\ \vdots & \vdots & \ddots \end{bmatrix} \begin{bmatrix} 1 + \rho_1 \rho_1 & \rho_1 \rho_2 & \cdots \\ \rho_2 \rho_1 & 1 + \rho_2 \rho_2 & \cdots \\ \vdots & \vdots & \ddots \end{bmatrix} \\ &= \begin{bmatrix} 1 - \sum O(\rho_a \rho_b \rho_c \rho_d) & \rho_1 \rho_2 - \rho_1 \rho_2 - \sum O(\rho_a \rho_b \rho_c \rho_d) & \cdots \\ -\rho_2 \rho_1 + \rho_2 \rho_1 - \sum O(\rho_a \rho_b \rho_c \rho_d) & 1 - \sum O(\rho_a \rho_b \rho_c \rho_d) & \cdots \\ \vdots & \vdots & \ddots \end{bmatrix} \approx \mathbf{I}. \end{aligned}$$

References

- T. Ajanthan, K. Gupta, P. Torr, R. Hartley, and P. Dokania. Mirror descent view for neural network quantization. In *International Conference on Artificial Intelligence and Statistics*, pages 2809–2817. PMLR, 2021.
- S.-i. Amari. *Information geometry and its applications*, volume 194. Springer, 2016.
- S.-i. Amari and H. Nagaoka. Methods of information geometry, volume 191 of translations of mathematical monographs, s. kobayashi and m. takesaki, editors. *American Mathematical Society, Providence, RI, USA*, pages 2–19, 2000.
- A. Appleton. Scalar curvature rigidity and ricci deturck flow on perturbations of euclidean space. *Calculus of Variations and Partial Differential Equations*, 57(5):1–23, 2018.
- J. L. Ba, J. R. Kiros, and G. E. Hinton. Layer normalization. *arXiv preprint arXiv:1607.06450*, 2016.
- Y. Bai, Y.-X. Wang, and E. Liberty. Proxquant: Quantized neural networks via proximal operators. *arXiv preprint arXiv:1810.00861*, 2018.
- R. H. Bamler. Stability of hyperbolic manifolds with cusps under ricci flow. *arXiv preprint arXiv:1004.2058*, 2010.

- R. H. Bamler. *Stability of Einstein metrics of negative curvature*. Princeton University, 2011.
- M. Basseville. Divergence measures for statistical data processing—an annotated bibliography. *Signal Processing*, 93(4):621–633, 2013.
- Y. Bengio, N. Léonard, and A. Courville. Estimating or propagating gradients through stochastic neurons for conditional computation. *arXiv preprint arXiv:1308.3432*, 2013.
- A. L. Besse. *Einstein manifolds*. Springer Science & Business Media, 2007.
- L. M. Bregman. The relaxation method of finding the common point of convex sets and its application to the solution of problems in convex programming. *USSR computational mathematics and mathematical physics*, 7(3):200–217, 1967.
- S. Bubeck et al. Convex optimization: Algorithms and complexity. *Foundations and Trends® in Machine Learning*, 8(3-4):231–357, 2015.
- Z. Cai, X. He, J. Sun, and N. Vasconcelos. Deep learning with low precision by half-wave gaussian quantization. In *Proceedings of the IEEE conference on computer vision and pattern recognition*, pages 5918–5926, 2017.
- J. Chen, L. Liu, Y. Liu, and X. Zeng. A learning framework for n-bit quantized neural networks toward fpgas. *IEEE Transactions on Neural Networks and Learning Systems*, pages 1–15, 2020. doi: 10.1109/TNNLS.2020.2980041.
- S. Chen, W. Wang, and S. J. Pan. Metaquant: Learning to quantize by learning to penetrate non-differentiable quantization. In *Advances in Neural Information Processing Systems*, volume 32, pages 3916–3926. Curran Associates, Inc., 2019.
- M. Courbariaux, I. Hubara, D. Soudry, R. El-Yaniv, and Y. Bengio. Binarized neural networks: Training deep neural networks with weights and activations constrained to+ 1 or-1. *arXiv preprint arXiv:1602.02830*, 2016.
- G. Cybenko. Approximation by superpositions of a sigmoidal function. *Mathematics of control, signals and systems*, 2(4):303–314, 1989.
- A. Deruelle and K. Kröncke. Stability of ale ricci-flat manifolds under ricci flow. *The Journal of Geometric Analysis*, 31(3):2829–2870, 2021.
- D. M. DeTurck. Deforming metrics in the direction of their ricci tensors. *Journal of Differential Geometry*, 18(1):157–162, 1983.
- B. Devyver. A gaussian estimate for the heat kernel on differential forms and application to the riesz transform. *Mathematische Annalen*, 358(1):25–68, 2014.
- T. Dozat. Incorporating nesterov momentum into adam. 2016.
- M. Elhoushi, Z. Chen, F. Shafiq, Y. H. Tian, and J. Y. Li. Deepshift: Towards multiplication-less neural networks. *arXiv preprint arXiv:1905.13298*, 2019.

- C. Guenther, J. Isenberg, and D. Knopf. Stability of the ricci flow at ricci-flat metrics. *Communications in Analysis and Geometry*, 10(4):741–777, 2002.
- P. Gysel, J. Pimentel, M. Motamedi, and S. Ghiasi. Ristretto: A framework for empirical study of resource-efficient inference in convolutional neural networks. *IEEE transactions on neural networks and learning systems*, 29(11):5784–5789, 2018.
- R. S. Hamilton et al. Three-manifolds with positive ricci curvature. *J. Differential geom.*, 17(2):255–306, 1982.
- K. He, X. Zhang, S. Ren, and J. Sun. Deep residual learning for image recognition. In *Proceedings of the IEEE conference on computer vision and pattern recognition*, pages 770–778, 2016.
- S. Helgason. *Differential geometry and symmetric spaces*, volume 341. American Mathematical Soc., 2001.
- G. Hinton. Neural networks for machine learning. coursera,[video lectures], 2012.
- K. Hornik. Approximation capabilities of multilayer feedforward networks. *Neural networks*, 4(2):251–257, 1991.
- L. Hou, Q. Yao, and J. T. Kwok. Loss-aware binarization of deep networks. *arXiv preprint arXiv:1611.01600*, 2016.
- A. G. Howard, M. Zhu, B. Chen, D. Kalenichenko, W. Wang, T. Weyand, M. Andreetto, and H. Adam. Mobilenets: Efficient convolutional neural networks for mobile vision applications. *arXiv preprint arXiv:1704.04861*, 2017.
- I. Hubara, M. Courbariaux, D. Soudry, R. El-Yaniv, and Y. Bengio. Binarized neural networks. In *Proceedings of the 30th International Conference on Neural Information Processing Systems*, pages 4114–4122, 2016.
- S. Ioffe and C. Szegedy. Batch normalization: Accelerating deep network training by reducing internal covariate shift. *arXiv preprint arXiv:1502.03167*, 2015.
- V. Jejjala, D. K. M. Pena, and C. Mishra. Neural network approximations for calabi-yau metrics. *arXiv preprint arXiv:2012.15821*, 2020.
- P. Kaul and B. Lall. Riemannian curvature of deep neural networks. *IEEE transactions on neural networks and learning systems*, 31(4):1410–1416, 2019.
- H. Koch and T. Lamm. Geometric flows with rough initial data. *Asian Journal of Mathematics*, 16(2):209–235, 2012.
- N. Koiso. Einstein metrics and complex structures. *Inventiones mathematicae*, 73(1):71–106, 1983.
- A. Krizhevsky, G. Hinton, et al. Learning multiple layers of features from tiny images. 2009.

- A. Krizhevsky, I. Sutskever, and G. E. Hinton. Imagenet classification with deep convolutional neural networks. In *Advances in neural information processing systems*, pages 1097–1105, 2012.
- O. A. Ladyzhenskaia, V. A. Solonnikov, and N. N. Ural'tseva. *Linear and quasi-linear equations of parabolic type*, volume 23. American Mathematical Soc., 1988.
- C. Leng, Z. Dou, H. Li, S. Zhu, and R. Jin. Extremely low bit neural network: Squeeze the last bit out with admm. In *Proceedings of the AAAI Conference on Artificial Intelligence*, volume 32, 2018.
- F. Li, B. Zhang, and B. Liu. Ternary weight networks. *arXiv preprint arXiv:1605.04711*, 2016.
- Z. Liu, B. Wu, W. Luo, X. Yang, W. Liu, and K.-T. Cheng. Bi-real net: Enhancing the performance of 1-bit cnns with improved representational capability and advanced training algorithm. In *Proceedings of the European conference on computer vision (ECCV)*, pages 722–737, 2018.
- C. Louizos, M. Reisser, T. Blankevoort, E. Gavves, and M. Welling. Relaxed quantization for discretized neural networks. In *International Conference on Learning Representations*, 2019. URL <https://openreview.net/forum?id=HkxjYoCqKX>.
- J. Martens. New insights and perspectives on the natural gradient method. *Journal of Machine Learning Research*, 21:1–76, 2020.
- V. Minerbe. Weighted sobolev inequalities and ricci flat manifolds. *Geometric and Functional Analysis*, 18(5):1696–1749, 2009.
- T. Pacini. Desingularizing isolated conical singularities: uniform estimates via weighted sobolev spaces. *arXiv preprint arXiv:1005.3511*, 2010.
- A. Paszke, S. Gross, F. Massa, A. Lerer, J. Bradbury, G. Chanan, T. Killeen, Z. Lin, N. Gimelshein, L. Antiga, et al. Pytorch: An imperative style, high-performance deep learning library. *arXiv preprint arXiv:1912.01703*, 2019.
- H. Qin, R. Gong, X. Liu, M. Shen, Z. Wei, F. Yu, and J. Song. Forward and backward information retention for accurate binary neural networks. In *Proceedings of the IEEE/CVF conference on computer vision and pattern recognition*, pages 2250–2259, 2020.
- M. Rastegari, V. Ordonez, J. Redmon, and A. Farhadi. Xnor-net: Imagenet classification using binary convolutional neural networks. In *European conference on computer vision*, pages 525–542. Springer, 2016.
- O. Russakovsky, J. Deng, H. Su, J. Krause, S. Satheesh, S. Ma, Z. Huang, A. Karpathy, A. Khosla, M. Bernstein, et al. Imagenet large scale visual recognition challenge. *International journal of computer vision*, 115(3):211–252, 2015.
- H. Sak, A. W. Senior, and F. Beaufays. Long short-term memory recurrent neural network architectures for large scale acoustic modeling. 2014.

- O. C. Schnürer, F. Schulze, and M. Simon. Stability of euclidean space under ricci flow. *arXiv preprint arXiv:0706.0421*, 2007.
- N. Sesum. Linear and dynamical stability of ricci-flat metrics. *Duke Mathematical Journal*, 133(1):1–26, 2006.
- N. Sheridan and H. Rubinstein. Hamilton’s ricci flow. *Honour thesis*, 2006.
- R. M. Wald. *General relativity*. University of Chicago press, 2010.
- J. Yang, X. Shen, J. Xing, X. Tian, H. Li, B. Deng, J. Huang, and X.-s. Hua. Quantization networks. In *Proceedings of the IEEE/CVF Conference on Computer Vision and Pattern Recognition (CVPR)*, June 2019.
- A. Zhou, A. Yao, Y. Guo, L. Xu, and Y. Chen. Incremental network quantization: Towards lossless cnns with low-precision weights. *arXiv preprint arXiv:1702.03044*, 2017.
- A. Zhou, A. Yao, K. Wang, and Y. Chen. Explicit loss-error-aware quantization for low-bit deep neural networks. In *Proceedings of the IEEE conference on computer vision and pattern recognition*, pages 9426–9435, 2018.
- S. Zhou, Y. Wu, Z. Ni, X. Zhou, H. Wen, and Y. Zou. Dorefa-net: Training low bitwidth convolutional neural networks with low bitwidth gradients. *arXiv preprint arXiv:1606.06160*, 2016.
- C. Zhu, S. Han, H. Mao, and W. J. Dally. Trained ternary quantization. *arXiv preprint arXiv:1612.01064*, 2016.
- F. Zhu, R. Gong, F. Yu, X. Liu, Y. Wang, Z. Li, X. Yang, and J. Yan. Towards unified int8 training for convolutional neural network. In *Proceedings of the IEEE/CVF Conference on Computer Vision and Pattern Recognition*, pages 1969–1979, 2020.